

Revisiting slepton pair production at the Large Hadron Collider

Benjamin Fuks,^{a,b} Michael Klasen,^c David R. Lamprea^c and Marcel Rothering^c

^a*Theory Division, Physics Department, CERN, CH-1211 Geneva 23, Switzerland*

^b*Institut Pluridisciplinaire Hubert Curien/Département Recherches Subatomiques, Université de Strasbourg/CNRS-IN2P3, 23 rue du Loess, F-67037 Strasbourg, France*

^c*Institut für Theoretische Physik, Westfälische Wilhelms-Universität Münster, Wilhelm-Klemm-Straße 9, D-48149 Münster, Germany*

E-mail: fuks@cern.ch, michael.klasen@uni-muenster.de,
david.lamprea@uni-muenster.de, marcel.rothering@uni-muenster.de

ABSTRACT: Motivated by the shift in experimental attention towards electroweak supersymmetric particle production at the CERN LHC, we update in this paper our precision predictions at next-to-leading order of perturbative QCD matched to resummation at the next-to-leading logarithmic accuracy for direct slepton pair production in proton-proton collisions. Simplified models, now commonly adopted by the experimental collaborations for selectrons and smuons as well as mixing staus, are used as benchmarks for total cross sections at achieved and future center-of-mass energies. They are presented together with the corresponding scale and parton density uncertainties in graphical and tabular form for future reference. Using modern Monte Carlo techniques, we also reanalyze recent ATLAS and CMS slepton searches in light of our precision cross sections and for various assumptions on the decomposition of the sleptons and their neutralino decay products.

KEYWORDS: Resummation, supersymmetry, hadron collider phenomenology, superparticle searches, electroweak superpartners

Contents

1	Introduction	1
2	Benchmark scenarios for slepton pair hadroproduction and decays	3
2.1	First and second generation sleptons	4
2.2	Simplified models for staus	5
3	Precision predictions for slepton pair production at the LHC	6
3.1	General features	6
3.2	Total cross section computations	9
3.3	Theoretical uncertainties	11
3.4	Summary tables	14
4	Sensitivity to slepton pair production at the LHC	15
4.1	Revisiting ATLAS searches for first and second generation sleptons	18
4.2	Revisiting CMS searches for first and second generation sleptons	21
5	Conclusion	24
A	Total cross sections at center-of-mass energies of 13 TeV and 14 TeV	25

1 Introduction

After almost fifty years of experimental tests, the Standard Model has proved to be a very successful theory of the fundamental particles and interactions. Nevertheless, it leaves many important questions, like the hierarchy of the fundamental mass scales, unanswered, and it is widely believed to represent a low-energy limit of a more fundamental theory. In particular, the recent discovery of a Higgs boson [1, 2], still to be confirmed as being *the* Standard Model Higgs boson, has rather reinforced our expectation to find physics beyond the Standard Model at the Large Hadron Collider (LHC) at CERN. This discovery is very likely the first observation of a particle intrinsically unstable with respect to quantum corrections, which requires either unnatural fine-tuning or stabilization from new particles lying around the TeV scale. This issue is addressed by large classes of new physics theories and in particular by weak-scale supersymmetry [3, 4], which also solves a considerable number of other problems inherent in the Standard Model. For instance, it hints at the possible unification of the gauge symmetries at high energies and provides a candidate particle explaining the presence of dark matter in the Universe.

As a consequence, searches for supersymmetry constitute one of the key topics of the present experimental program in high-energy particle physics. Up to now, both the ATLAS

and CMS collaborations have mainly focused on dedicated analyses of signatures arising from the strong production of squarks and gluinos, the partners of the strongly interacting quarks and gluons. However, no evidence for such particles has been found, so that squark and gluino masses are constrained to lie at higher and higher scales [5, 6]. The pair production of the electroweak superpartners, *i.e.*, the neutralino, chargino and slepton eigenstates, has therefore recently received more and more attention from both collaborations [7–16]. In addition, it has also been shown that the weak channels can be interesting probes for distinguishing minimal from non-minimal supersymmetry [17–21] and could also provide an explanation for the recent anomalous multilepton events observed by the CMS collaboration [22].

All these phenomenological and experimental studies so far rely on theoretical predictions valid either at the leading order [23–27] or at the next-to-leading order [28–31] of perturbative QCD, which may lead to large theoretical uncertainties. For more accurate predictions, and subsequently for more precise limits on or determination of the electroweak superpartner masses, the next-to-leading order results must be supplemented by QCD resummation, since soft-gluon radiation can give rise to large logarithmic terms that have to be resummed to all orders in the strong coupling constant [32–38]. In addition, a matching with fixed order computations is mandatory for consistent predictions in all kinematical regions.

Motivated by these observations, we have studied in a previous work resummation effects on chargino and neutralino pair production at the LHC for the already achieved center-of-mass energies of 7 TeV and 8 TeV [38]. Additionally, we have also very recently released a user-friendly computer code, dubbed RESUMMINO, allowing to perform such precision calculations for arbitrary supersymmetric scenarios and collision energies [39]. In this paper, we turn to slepton pair production and present accurate predictions for total cross sections at the LHC, focusing on benchmark scenarios based on simplified models as currently employed by both the ATLAS and CMS collaborations. We provide several cross section tables for LHC collisions at center-of-mass energies of 7 TeV, 8 TeV, 13 TeV and 14 TeV at the leading-order and next-to-leading order of perturbative QCD, and after matching the results with soft-gluon resummation. We also take the opportunity of performing a detailed study of the theoretical uncertainties, their control being largely improved by soft-gluon resummation. Including this information in the tables, we collect in this way the most precise cross section reference values so that they are available for all future ATLAS and CMS analyses of slepton pair production and decay.

In a second step, we reinterpret two of the most recent slepton LHC analyses. On the one hand, we include resummed predictions for total cross sections. On the other hand, we investigate the dependence of the predictions on the left-handed or right-handed nature of the slepton eigenstates, on its flavor, as well as on the bino, wino or higgsino nature of the lightest supersymmetric particle, assumed to be the lightest neutralino, which sleptons decay into. Experimental results indeed usually include either a sum over the slepton flavors or a sum over both slepton chiralities and focus on some specific neutralino decomposition. We demonstrate, in this work, that while the exact definition of the neutralino nature can be safely ignored, the expected limit strongly depends on the chosen patterns for the

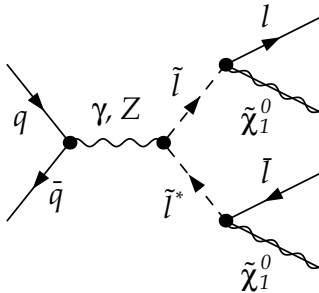


Figure 1. Leading-order Feynman diagram depicting slepton pair production and decay in the simplified models under consideration. The symbol $\tilde{\ell}$ stands for any generation of (s)leptons.

slepton nature. Therefore, making available results where only one specific slepton type is considered could be useful in the future, in particular when one aims for a recasting of the experimental analyses in the context of models where only one given slepton is light.

This work is organized as follows. In Section 2, we first describe a set of benchmark scenarios appropriate for slepton pair production studies. Next, we investigate in Section 3 slepton production cross sections and the corresponding scale and parton density function uncertainties. We then reinterpret, by means of state-of-the-art Monte Carlo simulations, two of the more recent slepton LHC analyses in Section 4 and focus on the variations of the results with respect to both precision predictions and the exact nature of the supersymmetric particles. Our results are summarized in Section 5, and in Appendix A we list total cross section expectations at next-to-leading logarithmic accuracy for future center-of-mass energies of 13 TeV and 14 TeV.

2 Benchmark scenarios for slepton pair hadroproduction and decays

In order to probe the usually large parameter spaces of several beyond the Standard Model theories simultaneously, simplified production and decay schemes have been developed. In this approach, model-independent search strategies are designed on the basis of models consisting of extensions of the Standard Model with minimal additions in terms of particles and interactions. These simplified models are constructed upon a very specific final state topology so that one can test generic features possibly common to several new physics models. Moreover, this framework aims for an easy comparison of theoretical predictions with data and reinterpretation of the experimental results in the case of complete theories.

In this section, we present two series of simplified models relevant for slepton pair production and decay at the LHC. Inspired by the constrained version of the Minimal Supersymmetric Standard Model (MSSM), sleptons $\tilde{\ell}$ are assumed to be light and always decay in a flavor-conserving way into the lightest supersymmetric particle, taken as the lightest neutralino $\tilde{\chi}_1^0$, and the corresponding Standard Model lepton ℓ . This pattern, illustrated in Figure 1, has motivated several experimental analyses where sleptons are

searched for in final states comprised of a same-flavor lepton pair produced in association with missing energy [10, 11, 15].

In the considered scenarios, the Standard Model is supplemented by two supersymmetric particles, a charged slepton $\tilde{\ell}$ and the lightest neutralino $\tilde{\chi}_1^0$, whereas the other supersymmetric particles are decoupled. This holds in particular for the strong superpartners associated with negative search results [5, 6]. The flavor and left-handed or right-handed nature of the considered slepton, together with the gaugino or higgsino nature of the lightest neutralino, allow us to define several series of benchmark scenarios which we describe in the rest of this section. First and second generation sleptons are addressed in Section 2.1, while third generation sleptons are considered in Section 2.2.

2.1 First and second generation sleptons

We start with the Standard Model field content and its $SU(3)_C \times SU(2)_L \times U(1)_Y$ gauge group. We then add a four-component Majorana spinor Ψ_N representing the lightest neutralino $\tilde{\chi}_1^0$ as well as one charged selectron or smuon field that we generically denote by $\tilde{\ell}_L$ or $\tilde{\ell}_R$. The L/R subscript refers to the chirality of the slepton Standard Model partner that is described by the Dirac field Ψ_ℓ . The associated Lagrangians are extracted from the MSSM Lagrangian and read, in the mass eigenbasis,

$$\begin{aligned} \mathcal{L}^{(L)} &= \mathcal{L}_{\text{SM}} + \partial_\mu \tilde{\ell}_L^\dagger \partial^\mu \tilde{\ell}_L + \frac{i}{2} \bar{\Psi}_N \gamma^\mu \partial_\mu \Psi_N + ie \left[\partial_\mu \tilde{\ell}_L^\dagger \tilde{\ell}_L - \tilde{\ell}_L^\dagger \partial_\mu \tilde{\ell}_L \right] A_\mu \\ &\quad - \frac{ie}{s_W c_W} \mathcal{C}_Z^{(L)} \left[\partial_\mu \tilde{\ell}_L^\dagger \tilde{\ell}_L - \tilde{\ell}_L^\dagger \partial_\mu \tilde{\ell}_L \right] Z_\mu + \left[\frac{1}{2c_W s_W} \bar{\Psi}_N \mathcal{C}_N^{(L)} P_L \Psi_\ell \tilde{\ell}_L^\dagger + \text{h.c.} \right], \\ \mathcal{L}^{(R)} &= \mathcal{L}_{\text{SM}} + \partial_\mu \tilde{\ell}_R^\dagger \partial^\mu \tilde{\ell}_R + \frac{i}{2} \bar{\Psi}_N \gamma^\mu \partial_\mu \Psi_N + ie \left[\partial_\mu \tilde{\ell}_R^\dagger \tilde{\ell}_R - \tilde{\ell}_R^\dagger \partial_\mu \tilde{\ell}_R \right] A_\mu \\ &\quad - \frac{ie}{s_W c_W} \mathcal{C}_Z^{(R)} \left[\partial_\mu \tilde{\ell}_R^\dagger \tilde{\ell}_R - \tilde{\ell}_R^\dagger \partial_\mu \tilde{\ell}_R \right] Z_\mu + \left[\frac{1}{2c_W s_W} \bar{\Psi}_N \mathcal{C}_N^{(R)} P_R \Psi_\ell \tilde{\ell}_R^\dagger + \text{h.c.} \right], \end{aligned} \quad (2.1)$$

for left-handed and right-handed sleptons, respectively. Additional interactions, such as four-scalar or neutralino-gauge interactions, are allowed by gauge invariance and supersymmetry. Moreover, contributions to the neutralino-lepton-slepton vertices proportional to the muon or electron Yukawa couplings are also present in the MSSM. However, in the context of the current work, these interactions are either phenomenologically irrelevant or negligibly small, so that they have been omitted for simplicity.

We have introduced, in the previous Lagrangians, the photon and Z -boson fields A_μ and Z_μ , the sine and cosine of the electroweak mixing angle s_W and c_W and the electromagnetic coupling constant e . Furthermore, in our conventions, the different coupling strengths are given by

$$\begin{aligned} \mathcal{C}_Z^{(L)} &= -\frac{1}{2} + s_W^2, \\ \mathcal{C}_N^{(L)} &= \sqrt{2}e \left[s_W N_1^* + c_W N_2^* \right], \\ \mathcal{C}_Z^{(R)} &= s_W^2, \\ \mathcal{C}_N^{(R)} &= -2\sqrt{2}e s_W N_1, \end{aligned} \quad (2.2)$$

where the complex quantities N_1 and N_2 stand for the bino and wino component of the lightest neutralino mass-eigenstate. For further reference, we denote the two higgsino components of the lightest neutralino by N_3 and N_4 , and the four mixing parameters are thus constrained by the unitarity relation

$$|N_1|^2 + |N_2|^2 + |N_3|^2 + |N_4|^2 = 1 . \quad (2.3)$$

This allows us to define a particular series of benchmark models as follows. First, the two parameters $M_{\tilde{\ell}}$ and $M_{\tilde{\chi}_1^0}$ representing the slepton and neutralino masses must be fixed, recalling that the neutralino has to be lighter than the slepton. Next, the flavor and chirality¹ of the slepton state have to be defined. Finally, it is also necessary to specify the gaugino/higgsino nature of the neutralino by fixing three of the four N_i quantities, the fourth one being derived by Eq. (2.3).

2.2 Simplified models for staus

In order to account for third generation sleptons, the simplified model described above has to be slightly modified. In contrast to the first two generations, the superpartners of the left-handed and right-handed taus are expected to mix as

$$\begin{pmatrix} \tilde{\tau}_1 \\ \tilde{\tau}_2 \end{pmatrix} = \begin{pmatrix} \cos \theta_{\tilde{\tau}} & \sin \theta_{\tilde{\tau}} \\ -\sin \theta_{\tilde{\tau}} & \cos \theta_{\tilde{\tau}} \end{pmatrix} \begin{pmatrix} \tilde{\tau}_L \\ \tilde{\tau}_R \end{pmatrix} , \quad (2.4)$$

where the mass eigenstates $\tilde{\tau}_1$ and $\tilde{\tau}_2$ are mass-ordered from the lighter to the heavier. Consequently, we focus on the production of the lightest of the two states, for which the associated cross section is larger.

To describe the interactions of the $\tilde{\tau}_1$ state, we construct a simplified model similarly to the one introduced in Section 2.1 and supplement the Standard Model with a state Ψ_N representing the lightest neutralino and a scalar field $\tilde{\tau}_1$ denoting the lighter supersymmetric partner of the tau lepton, described by the Dirac spinor Ψ_τ . The associated Lagrangian reads

$$\begin{aligned} \mathcal{L}^{(\tau)} = & \mathcal{L}_{\text{SM}} + \partial_\mu \tilde{\tau}_1^\dagger \partial^\mu \tilde{\tau}_1 + \frac{i}{2} \bar{\Psi}_N \gamma^\mu \partial_\mu \Psi_N \\ & + ie \left[\partial_\mu \tilde{\tau}_L^\dagger \tilde{\tau}_1 - \tilde{\tau}_1^\dagger \partial_\mu \tilde{\tau}_1 \right] A_\mu - \frac{ie}{s_W c_W} \mathcal{C}_Z^{(\tau)} \left[\partial_\mu \tilde{\tau}_1^\dagger \tilde{\tau}_1 - \tilde{\tau}_1^\dagger \partial_\mu \tilde{\tau}_1 \right] Z_\mu \\ & + \frac{1}{2c_W s_W} \left[\bar{\Psi}_N \mathcal{C}_N^{(\tau,L)} P_L \Psi_\tau \tilde{\tau}_1^\dagger + \bar{\Psi}_N \mathcal{C}_N^{(\tau,R)} P_R \Psi_\tau \tilde{\tau}_1^\dagger + \text{h.c.} \right] , \end{aligned} \quad (2.5)$$

where we have again omitted all the interactions irrelevant for stau pair production and decay at the LHC. The Lagrangian parameters can be deduced from Eq. (2.2) after accounting for appropriate gauge-eigenstate mixings,

$$\begin{aligned} \mathcal{C}_Z^{(\tau)} &= \left[-\frac{1}{2} + s_W^2 \right] \cos^2 \theta_{\tilde{\tau}} + \left[s_W^2 \right] \sin^2 \theta_{\tilde{\tau}} , \\ \mathcal{C}_N^{(\tau,L)} &= \sqrt{2}e \left[s_W N_1^* + c_W N_2^* \right] \cos \theta_{\tilde{\tau}} - \left[2c_W s_W N_3^* y_\tau \right] \sin \theta_{\tilde{\tau}} , \\ \mathcal{C}_N^{(\tau,R)} &= \left[-2\sqrt{2}e s_W N_1 \right] \sin \theta_{\tilde{\tau}} - \left[2c_W s_W N_3 y_\tau \right] \cos \theta_{\tilde{\tau}} , \end{aligned} \quad (2.6)$$

¹Strictly speaking, a scalar field has no chirality and we always refer to the chirality of the Standard Model partner.

where y_τ denotes the tau lepton Yukawa coupling, which in this case cannot be neglected.

Simplified models describing tau sleptons are thus defined by two mass parameters, namely the lightest stau and lightest neutralino masses $M_{\tilde{\tau}_1}$ and $M_{\tilde{\chi}_1^0}$, three out of the four neutralino mixing parameters (the N_i quantities) as well as the stau mixing angle $\theta_{\tilde{\tau}}$. The fourth neutralino component is again extracted using Eq. (2.3).

3 Precision predictions for slepton pair production at the LHC

In this section, we present total cross sections relevant for direct slepton searches as performed by the ATLAS and CMS experiments. We focus on both past LHC runs at center-of-mass energies of 7 TeV and 8 TeV, while results for possible future runs at center-of-mass energies of 13 TeV and 14 TeV are presented in Appendix A. Further predictions can be made available by employing the RESUMMINO package [39], that can be downloaded from the webpage

<http://www.resummino.org>

or be obtained from the authors upon request.

3.1 General features

In the pioneering and subsequent more recent works, slepton pair production has been studied at the leading-order [23–25] and next-to-leading order [29] of perturbative QCD. All of these cross section calculations rely on the QCD factorization theorem. Rendering the dependence on the slepton-pair invariant mass M explicit, the results are obtained by convoluting the partonic cross section $d\hat{\sigma}_{ab}$ with the universal distribution functions f_a and f_b of partons a and b carrying the momentum fractions x_a and x_b of the colliding hadrons,

$$M^2 \frac{d\sigma}{dM^2}(\tau) = \sum_{ab} \int_0^1 dx_a dx_b dz \delta(\tau - x_a x_b z) \left[x_a f_a(x_a, \mu_F^2) \right] \left[x_b f_b(x_b, \mu_F^2) \right] \times \left[z d\hat{\sigma}_{ab}(z, M^2, \mu_F^2, \mu_R^2) \right]. \quad (3.1)$$

In this equation, μ_R and μ_F stand for the factorization and renormalization scales and $\tau = M^2/S$, \sqrt{S} being the hadronic center-of-mass energy. Although the partonic cross section $d\hat{\sigma}_{ab}$ exhibits logarithmic terms that are large close to the production threshold, $z \lesssim 1$, the convergence of the perturbative series is recovered at the hadronic level thanks to the vanishing parton densities when the momentum fraction is close to one. This however yields significant scale uncertainties making the theoretical predictions less precise.

These logarithmic terms are not surprising and originate from soft and collinear radiation of partons by the initial state particles. It has been proved long ago that in this case, once transformed into the appropriate conjugate space, the cross section can be refactored. Consequently, the large logarithms can be resummed to all orders in the strong coupling, which implies an important reduction of the theoretical uncertainties by including in the predictions higher order effects in a consistent way. More specifically, this threshold resummation formalism is based on the fact that we can write the cross section, in the

conjugate Mellin N -space, as

$$M^2 \frac{d\sigma}{dM^2}(N-1) = \sum_{ab} f_a(N, \mu_F^2) f_b(N, \mu_F^2) \hat{\sigma}_{ab}(N, M^2, \mu_F^2, \mu_R^2), \quad (3.2)$$

where the Mellin N -moments of the quantities $F = \sigma$, $\hat{\sigma}_{ab}$ and $f_{a,b}$ are given, in our conventions, by

$$F(N) = \int_0^1 dy y^{N-1} F(y), \quad (3.3)$$

with $y = \tau$, z and $x_{a,b}$, respectively. Reorganizing the different contributions to the partonic cross section, the latter can be recast in a closed exponential form [40–51],

$$\hat{\sigma}_{ab}(N, M^2, \mu_F^2, \mu_R^2) = \mathcal{H}_{ab}(M^2, \mu_F^2, \mu_R^2) \exp \left[\mathcal{G}_{ab}(N, M^2, \mu_F^2, \mu_R^2) \right]. \quad (3.4)$$

This expression contains two functions, the hard function \mathcal{H} and the Sudakov form factor \mathcal{G} . The hard function can be derived from the perturbative results by first isolating the terms independent of the Mellin variable N and then collecting the dominant $1/N$ -terms stemming from universal collinear radiation of the initial state partons. In contrast, the Sudakov form factor embeds the dominant dependence on N , *i.e.*, it contains soft and collinear parton emission and absorbs in this way all large logarithmic contributions. For more details on the explicit form of the \mathcal{H} and \mathcal{G} functions, we refer to Ref. [39].

Far from threshold, the perturbative computation, only partially accounted for in Eq. (3.4), is expected to be reliable. Therefore, predictions valid in all kinematical regions require a consistent matching of the fixed order with the resummed results. This is achieved by subtracting from the sum of both predictions their overlap calculated by expanding analytically the resummed cross section at the same order in the strong coupling as the one employed for the fixed order calculation.

Finally, contrary to the fixed order results that are computed in physical space using Eq. (3.1), the resummed component and its expansion at a given order are evaluated in Mellin space. Therefore, it is necessary to transform them back to the physical space. Care must be taken with the singularities possibly arising at the level of the N -space cross section. To this aim, we choose an integration contour inspired by the principal value procedure and the minimal prescription [52, 53], which satisfies two properties. First, the poles associated with the Regge singularity of the Mellin moments of the parton densities lie to the left of the integration contour. Second, the Landau pole related to the running of the strong coupling lies to its right.

Threshold resummation has been initially performed in the context of slepton pair production several years ago. This computation combines soft gluon resummation at the next-to-leading logarithmic accuracy and a fixed order calculation at the next-to-leading order [33]. It should be noted that soft gluon resummation can also be performed when the transverse momentum of the produced slepton pair p_T is small [32], as this gives also rise to possibly large logarithmic terms, or simultaneously in both regimes, *i.e.*, when p_T is small and M close to threshold [34].

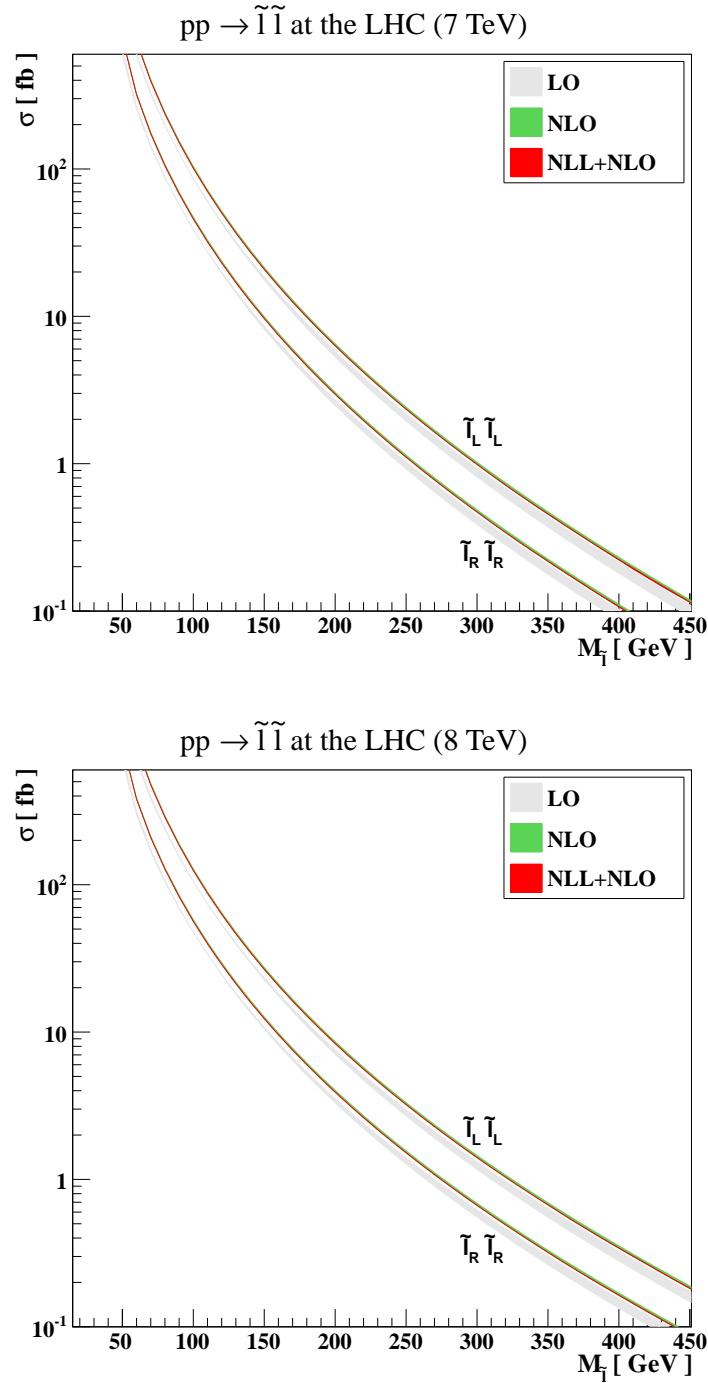


Figure 2. Total cross sections for slepton pair production at the LHC, running at center-of-mass energies of 7 TeV (upper panel) and 8 TeV (lower panel). We present predictions as functions of the slepton mass $M_{\tilde{l}}$ at LO (gray) and NLO (green) of perturbative QCD and after matching the NLO results with threshold resummation at the NLL accuracy (red). The uncertainty bands correspond to variations induced by modifications of the unphysical scales in the $[1/2M_{\tilde{l}}, 2M_{\tilde{l}}]$ range.

3.2 Total cross section computations

We dedicate this section to an overview of the behavior of the total rate for slepton pair production at the LHC as a function of the slepton mass $M_{\tilde{\ell}}$. We fix Fermi’s coupling constant and the masses and widths of the electroweak gauge bosons to their latest measured values [54] and compute the squared sine of the electroweak mixing angle and the electromagnetic fine structure constant in the improved Born approximation. We then numerically evaluate total cross section predictions at the leading order (LO) and next-to-leading order (NLO) of perturbative QCD, and after matching the NLO results with a computation including the resummation of the threshold logarithms at the next-to-leading logarithmic accuracy (NLL+NLO). Focusing on both past runs of the LHC, we present results for the series of benchmark models introduced in Section 2.1 in Figure 2 for collider center-of-mass energies of 7 TeV (upper panel of the figure) and 8 TeV (lower panel of the figure). While the LO predictions are obtained after convoluting the partonic results with the leading order fit of the CTEQ6 parton densities [55], we employ the more recent NLO CT10 fit of the CTEQ collaboration [56] for our NLO and NLL+NLO calculations. In all cases, both factorization and renormalization scales are fixed to the mass of the produced slepton $\mu_R = \mu_F = M_{\tilde{\ell}}$.

We present, in Figure 2, results for a restricted slepton mass range of $M_{\tilde{\ell}} \in [0, 450]$ GeV, which corresponds to parameter space regions where cross sections of at least about 0.1 fb are expected for both the pair production of left-handed and right-handed slepton pairs. Equivalently, in the case a supersymmetric model with light sleptons is realized in Nature, those regions feature the presence of at least a few slepton events in the 2011-2012 LHC data, although these events are hidden in an overwhelming Standard Model background. Furthermore, cross sections greater than about 10 fb are found for left-handed (right-handed) sleptons whose mass satisfies $M_{\tilde{\ell}} \lesssim 200$ GeV (150 GeV), so that the corresponding benchmark scenarios are appealing models for the possible observation of hints for sleptons at the LHC. This is addressed more into details in Section 4.

In addition, Figure 2 also shows that large K -factors are obtained when including NLO corrections to the predictions, reaching up to 1.25 in the low-mass region ($M_{\tilde{\ell}} \gtrsim 50$ GeV) and 1.15 for heavier sleptons ($M_{\tilde{\ell}} \gtrsim 200$ GeV). Matching the NLO results to a computation including the threshold resummation of the soft gluon radiation at the NLL accuracy does not drastically modify the NLO K -factor, although theoretical uncertainties estimated by varying the unphysical scales by a factor of two around the central scale, chosen to be the mass of the produced sleptons, are found to be largely reduced. This property is addressed in greater detail in Section 3.3.

In Figure 3, we investigate stau pair production in the framework of the simplified models introduced in Section 2.2. We show the dependence of the total cross section, computed after matching the resummed results with the NLO predictions for both LHC center-of-mass energies of 7 TeV (upper panel of the figure) and 8 TeV (lower panel of the figure), on both the stau mass $M_{\tilde{\tau}_1}$ and the sine of the mixing angle $\sin\theta_{\tilde{\tau}}$. As before, we convolute the partonic cross sections with the CT10 NLO parton distribution functions (PDFs) and fix the unphysical scales to the mass of the produced stau eigenstate $\mu_F =$

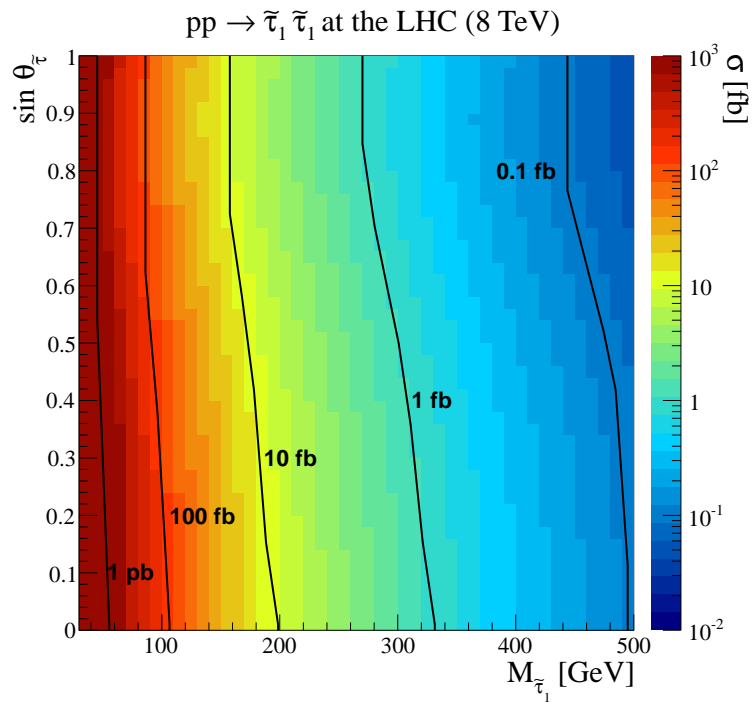
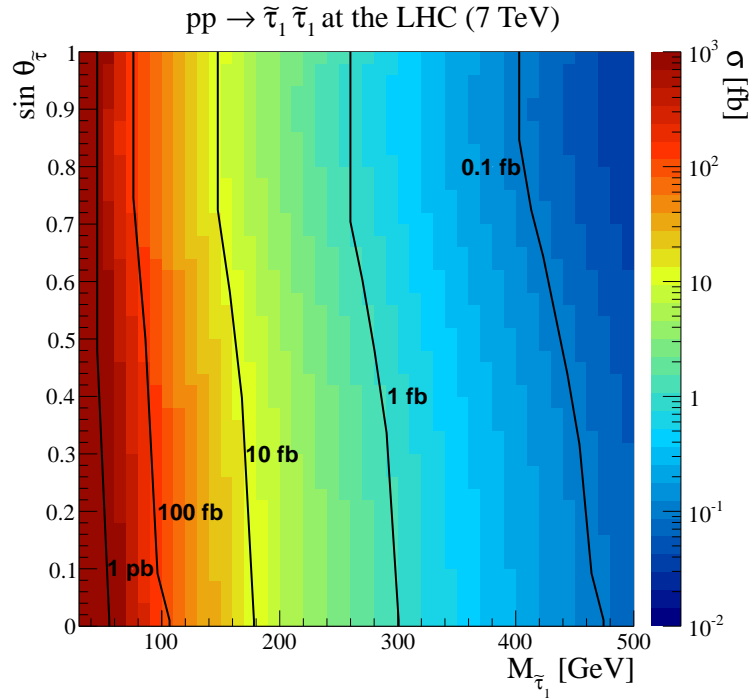


Figure 3. Total cross sections for stau pair production at the LHC, running at center-of-mass energies of 7 TeV (upper panel) and 8 TeV (lower panel). We present predictions as functions of the stau mass and the stau mixing angle after matching the NLO results with threshold resummation at the NLL accuracy.

$\mu_R = M_{\tilde{\tau}_1}$. Similarly to the first and second generation slepton cases, cross sections larger than about 10 fb are obtained for stau masses ranging up to about 150 – 200 GeV for both center-of-mass energies. However, from the perspective of the possible observation of stau events at the LHC, the situation is expected to be more complicated due to tau reconstruction efficiencies. We refer to Section 4 for more details.

As already found for smuon and selectron pair production, total cross sections associated with the production of a pair of left-handed sfermions are larger than those related to the production of a pair of right-handed sfermions. Stau eigenstates mainly constituted of a left-handed component are therefore more easily produced than when the right-handed component is dominant. In the rest of this paper, we adopt a scenario where the stau mixing is maximal, *i.e.*, $\theta_{\tilde{\tau}} = \pi/4$. One observes in Figure 3 that this implies a cross section value almost minimal for stau lighter than 200 GeV and slightly larger than the minimal value for heavier staus. A large mixing can however allow for sizable loop-induced contributions to stau pair production from bottom-antibottom or gluon-pair initial states [57]. This has not been considered in the present work.

3.3 Theoretical uncertainties

In the previous subsection, we have briefly mentioned that slepton pair production total cross section predictions are stabilized with respect to scale variations when resummation techniques are employed. The NLL+NLO prediction have indeed been found much less dependent on the common unphysical scale $\mu_R = \mu_F = M_{\tilde{\ell}}$ than the LO and NLO expectations, where the central scale value is taken as the mass of the produced sleptons. In this section, we investigate this property more into detail and show, in Figure 4, the scale dependence of the total cross sections for different subprocesses, a slepton mass fixed to 300 GeV and a center-of-mass energy of 8 TeV. We separately consider variations of the renormalization (upper panel of the figure) and factorization (lower panel of the figure) scale for the production of a left-handed first or second generation slepton pair, a right-handed first or second generation slepton pair and for a stau pair where the stau is defined as a maximal admixture of the left-handed and right-handed stau gauge-eigenstates.

As mentioned above, we fix, on the upper panel of the figure, the factorization scale to its central value, $\mu_F = M_{\tilde{\ell}} = 300$ GeV, and vary the renormalization scale μ_R by a factor of four around this value. We study the dependence of the total rate, as a function of the ratio $\mu_R/M_{\tilde{\ell}}$, at LO and NLO of perturbative QCD and after matching the NLO results with resummation predictions at the NLL accuracy. As the tree-level Feynman diagrams do not exhibit any QCD vertex, the LO predictions are independent of the renormalization scale μ_R . In contrast, logarithms of the renormalization scale appear at higher orders through the strong coupling constant $\alpha_s(\mu_R)$ entering in both virtual loop-diagrams and real emission diagrams, which makes the NLO and NLL+NLO results depending on μ_R . The NLO cross sections hence decrease with increasing values of the renormalization scale, whilst at the NLL accuracy, the resummation of soft gluon emissions attenuates this dependence, increasing the size of the plateau region.

On the lower panel of Figure 4, we conversely fix the renormalization scale to its central value $\mu_R = M_{\tilde{\ell}} = 300$ GeV and vary the factorization scale μ_F by a factor of four around this

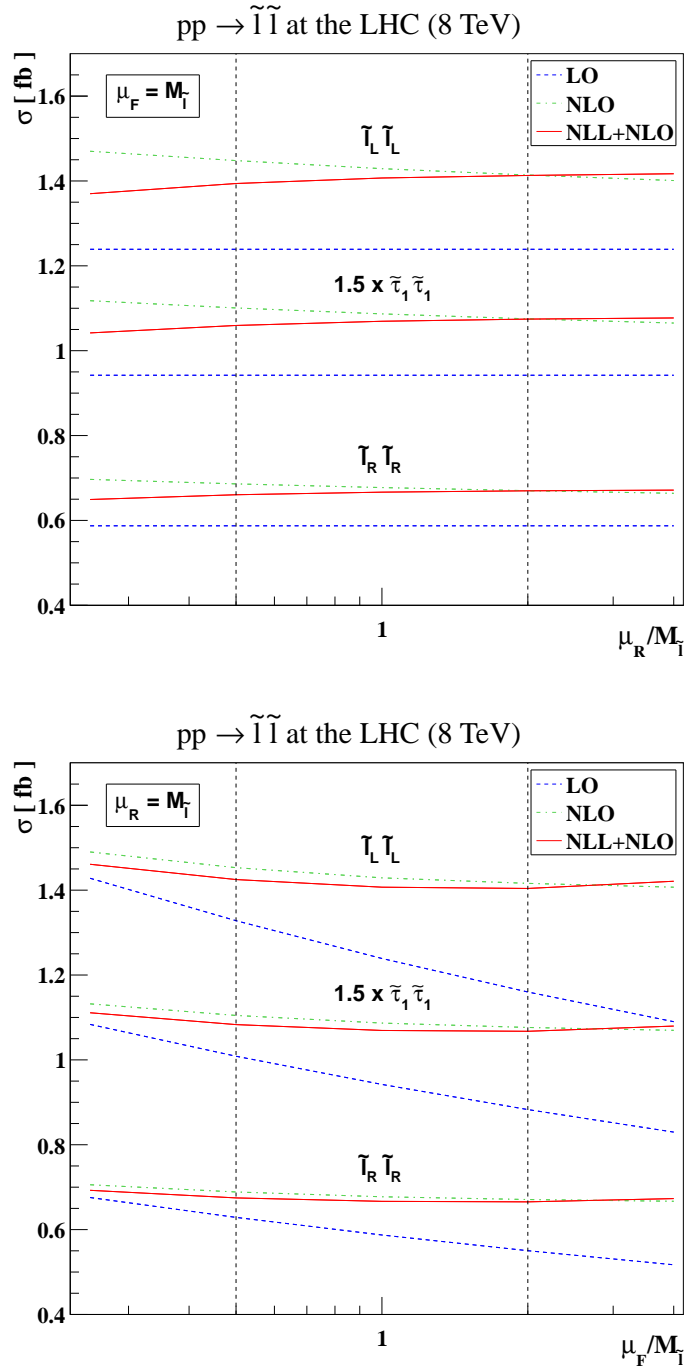


Figure 4. Total cross sections for the production of a pair of left-handed first or second generation sleptons, right-handed first or second generation sleptons and maximally mixing staus at the LHC, running at a center-of-mass energy of 8 TeV. We depict the dependence of the results on the renormalization (upper panel) and factorization (lower panel) scales at the LO (dashed blue), NLO (dashed-dotted green) and NLL+NLO (plain red) accuracy.

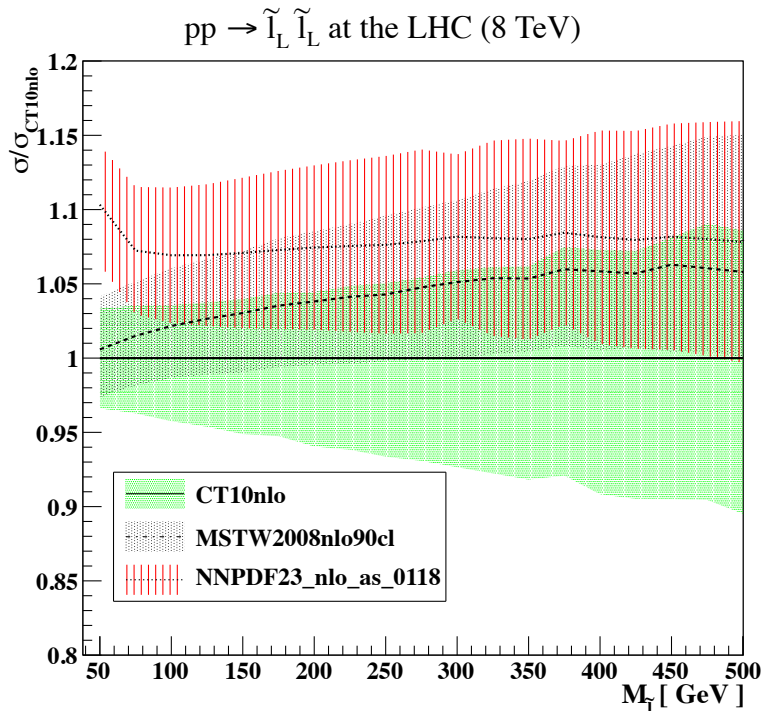


Figure 5. Total cross sections for the production of a pair of left-handed sleptons at the LHC, running at a center-of-mass energy of 8 TeV. We study the dependence of the results on the parton density fits by showing predictions obtained with the central PDF fits as provided by the CTEQ (plain), MSTW (dashed) and NNPDF (dotted) collaborations, normalized to results obtained when using the best CT10 NLO fit. We indicate additionally the associated theoretical uncertainties for all PDF choices.

value, the results being presented as functions of the ratio $\mu_F/M_{\tilde{l}}$. The LO estimates of the cross sections feature a very strong dependence on the factorization scale, in particular due to the employed leading order set of parton densities [55]. Using instead parton densities including NLO corrections in their evolution and extracted by making use of more precise Standard Model predictions [56] allows to largely tame this dependence², which is even further reduced with soft gluon resummation although the same PDF sets are employed.

We now study another source of theoretical uncertainties for cross section predictions and investigate the dependence of the results on the choice of the parton density fits. Up to now, we have computed NLL+NLO cross sections using the best NLO fit provided by the CTEQ collaboration, dubbed CT10 [56]. In order to assess the uncertainties arising from this choice, we re-evaluate the total rate for slepton pair production at the LHC using each of the 52 parton density fits accompanying the CT10 best fit, which allows to estimate the effects of $\pm 1\sigma$ variations along the $n = 26$ eigenvectors of the parton density fit covariance matrix. The positive and negative variations $\Delta\sigma_{\text{up}}$ and $\Delta\sigma_{\text{down}}$ from the central cross

²A part of the effects is induced by the partonic cross sections which depend on both μ_R and μ_F at NLO and NLL+NLO.

section value σ_0 are then computed by combining the 52 results,

$$\begin{aligned}\Delta\sigma_{\text{up}} &= \sqrt{\sum_{i=1}^n \left[\max(\sigma_{+i} - \sigma_0, \sigma_{-i} - \sigma_0, 0) \right]^2}, \\ \Delta\sigma_{\text{down}} &= \sqrt{\sum_{i=1}^n \left[\max(\sigma_0 - \sigma_{+i}, \sigma_0 - \sigma_{-i}, 0) \right]^2},\end{aligned}\tag{3.5}$$

where σ_{+i} and σ_{-i} denote predictions obtained when employing a PDF set including a positive and negative variation along the i^{th} eigenvector of the covariance matrix, respectively. We finally compare the obtained cross section envelope to the ones obtained when making use of the 90% confidence level MSTW 2008 parton density fit [58] and of the 2.3 version of the NNPDF fit [59, 60]. In the first case, the uncertainties $\Delta\sigma_{\text{up}}$ and $\Delta\sigma_{\text{down}}$ are computed as above while in the latter case, we extract the 2σ range spanned by the 100 replica fits provided with the NNPDF set. As NNPDF densities cannot be properly transformed in Mellin space, the method described in Section 3.1 is not appropriate. We instead rely, for a fixed slepton mass, on the ratio κ of the NLL+NLO to NLO results which is expected to be largely independent of the parton density choice if the two calculations employ PDF sets evaluated at the same perturbative order. This feature has been verified with the CT10 and MSTW 2008 densities. Therefore, the NNPDF results at the NLL+NLO accuracy are based on a pure NLO computation, rescaled by the average κ value obtained when considering all CT10 or MSTW 2008 PDF sets.

The results are presented in Figure 5, where we focus on the production of a pair of left-handed sleptons at the LHC running at a center-of-mass energy of 8 TeV and study the dependence of the predictions on different choices for the slepton mass. We normalize the NLL+NLO predictions to the rate obtained when using the best NLO PDF fit provided by the CTEQ collaboration and include the uncertainties as defined above for the CT10, MSTW 2008 and NNPDF 2.3 fits. We observe that up to these uncertainties, all predictions agree over the covered slepton mass range at the percent level. However, while the theoretical errors associated with the production of a pair of light sleptons are of a few percents, they increase with the slepton mass, reaching about 10% for 500 GeV sleptons. This is due to the relevant regions of the (x, μ_F^2) parameter space that lead to PDFs less constrained by data when the slepton mass increases.

3.4 Summary tables

We summarize all the results computed in this section in Table 1 and Table 2 where we provide slepton pair production cross sections at the LHC, running at a center-of-mass energy of 7 TeV and 8 TeV, respectively, for different choices of the produced superparticle masses and nature. We separately consider, in the framework of the series of benchmark scenarios described in Section 2.1, the production of left-handed and right-handed first or second generation sleptons, together with the production of a pair of maximally mixing staus in the context of benchmark scenarios as introduced in Section 2.2. We additionally indicate theoretical uncertainties induced by variations of the unphysical scales $\mu_R = \mu_F$ by

a factor of two around the central scale value taken as the mass of the produced sleptons, as well as those related to variations along the 26 eigenvectors of the covariance matrix associated with the CT10 parton density fit which we compute as presented in Section 3.3.

4 Sensitivity to slepton pair production at the LHC

Until recently, both LHC collaborations were mainly focusing on searches for the strongly interacting superpartners. As a consequence of the associated negative search results, the interest in the production of the electroweak superpartners, and in particular in the production of a pair of charged sleptons, has increased over the last few years. Dedicated direct slepton ATLAS and CMS analyses have hence allow one to improve, for the first time from the end of LEP experiments, the bounds on the slepton masses.

We dedicate this section to the reinterpretation of the recent ATLAS results of Ref. [7] and CMS results of Ref. [15]. These two analyses both contain a signal region focusing on final states featuring an electron-positron or muon-antimuon pair produced in association with missing transverse energy. They are therefore suitable for the extraction of bounds on the first and second generation sleptons from their direct pair production at the LHC, followed by their subsequent decays into the corresponding Standard Model partner and missing energy. The limits on the slepton masses obtained from those analyses have been initially deduced after considering simplified models such as those introduced in Section 2.1 but under a very specific setup in terms of the nature of the sleptons and neutralinos. In Section 4.1 and Section 4.2, we generalize these results in the context of arbitrary neutralino (bino, wino or mixed bino-wino³) and slepton (left-handed or right-handed) compositions, and also study their dependence on the slepton flavor.

The ATLAS analysis of Ref. [10] is based on the production of two hadronically-decaying taus with missing energy, so that it could be in principle recast in the context of the production of a pair of staus in the framework of any of the benchmark scenario of the class of simplified models designed in Section 2.2. However, a complicated tau reconstruction together with small signal cross sections, in particular once we include the tau decay branching ratios, render the task of constraining the simplified model parameter space impossible. This would indeed requires cross sections larger by at least factors of 10-50 in the best cases (*i.e.*, in the low mass region of the parameter space) in order to imply at least a few visible events assuming the currently available luminosity.

In order to simulate signal events at the LHC, we employ the Monte Carlo event generator MADGRAPH 5 [61] and use its interface to PYTHIA 6 [62] to generate hadron-level events from the merging of parton-level events associated with matrix elements containing up to two additional hard jets [63–65]. While the TAUOLA [66] package is employed for the handling of tau decays, detector simulation is performed by means of the DELPHES program [67], using the recent CMS detector description of Ref. [68] and the built-in ATLAS detector setup. The simplified scenarios that have been designed in Section 2 have been implemented in MADGRAPH 5 via the UFO interface [69] of FEYNRULES [70–74] and the

³Due to the negligible first and second generation Yukawa couplings, selectrons and smuons do not couple to the Higgsino components of the neutralinos that are therefore not considered.

$M_{\tilde{\ell}}$ [GeV]	Final state	LO [fb]	NLO [fb]	NLL+NLO [fb]
50	$\tilde{\ell}_L^+ \tilde{\ell}_L^-$	$1381.00^{+6.8\%}_{-27.4\%}$	$1740.00^{+16.4\%+3.2\%}_{-1.4\%-4.5\%}$	$1723.00^{-0.6\%+3.2\%}_{-0.1\%-4.5\%}$
	$\tilde{\ell}_R^+ \tilde{\ell}_R^-$	$619.40^{+6.9\%}_{-27.4\%}$	$780.80^{+16.4\%+3.4\%}_{-1.5\%-4.5\%}$	$773.30^{-0.6\%+3.4\%}_{-0.1\%-4.5\%}$
	$\tilde{\tau}_1^+ \tilde{\tau}_1^-$	$407.20^{+5.9\%}_{-28.1\%}$	$512.90^{+17.0\%+3.9\%}_{-1.3\%-4.9\%}$	$506.90^{-0.6\%+3.9\%}_{-0.1\%-4.9\%}$
100	$\tilde{\ell}_L^+ \tilde{\ell}_L^-$	$85.97^{+0.8\%}_{-22.1\%}$	$102.60^{+16.0\%+3.5\%}_{-1.9\%-4.7\%}$	$101.20^{+0.3\%+3.5\%}_{-0.2\%-4.7\%}$
	$\tilde{\ell}_R^+ \tilde{\ell}_R^-$	$38.88^{+0.8\%}_{-22.2\%}$	$46.42^{+16.0\%+4.0\%}_{-1.8\%-5.1\%}$	$45.80^{+0.3\%+4.0\%}_{-0.3\%-5.1\%}$
	$\tilde{\tau}_1^+ \tilde{\tau}_1^-$	$39.82^{+0.8\%}_{-22.2\%}$	$47.53^{+16.0\%+4.1\%}_{-1.9\%-5.3\%}$	$46.88^{+0.3\%+4.1\%}_{-0.3\%-5.3\%}$
150	$\tilde{\ell}_L^+ \tilde{\ell}_L^-$	$18.06^{+3.4\%}_{-19.8\%}$	$21.13^{+11.6\%+4.0\%}_{-2.0\%-5.6\%}$	$20.80^{+0.5\%+4.0\%}_{-0.2\%-5.6\%}$
	$\tilde{\ell}_R^+ \tilde{\ell}_R^-$	$8.37^{+3.3\%}_{-19.9\%}$	$9.79^{+11.7\%+4.4\%}_{-2.0\%-6.3\%}$	$9.64^{+0.5\%+4.4\%}_{-0.2\%-6.3\%}$
	$\tilde{\tau}_1^+ \tilde{\tau}_1^-$	$8.81^{+3.3\%}_{-19.8\%}$	$10.31^{+11.7\%+4.7\%}_{-1.9\%-6.2\%}$	$10.16^{+0.6\%+4.7\%}_{-0.2\%-6.2\%}$
200	$\tilde{\ell}_L^+ \tilde{\ell}_L^-$	$5.52^{+5.0\%}_{-18.9\%}$	$6.40^{+9.1\%+4.5\%}_{-1.9\%-6.5\%}$	$6.30^{+0.7\%+4.5\%}_{-0.0\%-6.5\%}$
	$\tilde{\ell}_R^+ \tilde{\ell}_R^-$	$2.59^{+4.9\%}_{-18.9\%}$	$3.00^{+9.2\%+5.2\%}_{-1.9\%-7.1\%}$	$2.95^{+0.3\%+5.2\%}_{-0.0\%-7.1\%}$
	$\tilde{\tau}_1^+ \tilde{\tau}_1^-$	$2.75^{+4.9\%}_{-18.9\%}$	$3.19^{+9.2\%+5.3\%}_{-1.9\%-7.2\%}$	$3.14^{+0.7\%+5.3\%}_{-0.0\%-7.2\%}$
250	$\tilde{\ell}_L^+ \tilde{\ell}_L^-$	$2.06^{+6.2\%}_{-18.5\%}$	$2.38^{+7.5\%+5.1\%}_{-1.8\%-7.3\%}$	$2.34^{+0.7\%+5.1\%}_{-0.0\%-7.3\%}$
	$\tilde{\ell}_R^+ \tilde{\ell}_R^-$	$0.97^{+6.1\%}_{-18.5\%}$	$1.12^{+7.6\%+6.0\%}_{-1.8\%-7.8\%}$	$1.10^{+0.8\%+6.0\%}_{-0.0\%-7.8\%}$
	$\tilde{\tau}_1^+ \tilde{\tau}_1^-$	$1.04^{+6.1\%}_{-18.5\%}$	$1.20^{+7.7\%+5.9\%}_{-1.8\%-8.0\%}$	$1.18^{+0.8\%+5.9\%}_{-0.0\%-8.0\%}$
300	$\tilde{\ell}_L^+ \tilde{\ell}_L^-$	$0.87^{+7.1\%}_{-18.6\%}$	$1.00^{+6.5\%+5.8\%}_{-2.1\%-8.0\%}$	$0.99^{+0.9\%+5.8\%}_{-0.1\%-8.0\%}$
	$\tilde{\ell}_R^+ \tilde{\ell}_R^-$	$0.41^{+7.1\%}_{-18.5\%}$	$0.48^{+6.6\%+6.7\%}_{-2.0\%-8.8\%}$	$0.47^{+0.7\%+6.7\%}_{-0.0\%-8.8\%}$
	$\tilde{\tau}_1^+ \tilde{\tau}_1^-$	$0.44^{+7.0\%}_{-18.6\%}$	$0.51^{+6.6\%+6.7\%}_{-2.0\%-8.9\%}$	$0.50^{+0.8\%+6.7\%}_{-0.1\%-8.9\%}$
350	$\tilde{\ell}_L^+ \tilde{\ell}_L^-$	$0.40^{+7.9\%}_{-18.9\%}$	$0.46^{+5.8\%+6.5\%}_{-2.2\%-8.8\%}$	$0.45^{+1.0\%+6.5\%}_{-0.2\%-8.8\%}$
	$\tilde{\ell}_R^+ \tilde{\ell}_R^-$	$0.19^{+7.8\%}_{-18.8\%}$	$0.22^{+5.9\%+7.5\%}_{-2.1\%-9.8\%}$	$0.22^{+1.0\%+7.5\%}_{-0.2\%-9.8\%}$
	$\tilde{\tau}_1^+ \tilde{\tau}_1^-$	$0.20^{+7.8\%}_{-18.8\%}$	$0.24^{+5.9\%+7.7\%}_{-2.1\%-9.8\%}$	$0.23^{+1.0\%+7.7\%}_{-0.3\%-9.8\%}$
400	$\tilde{\ell}_L^+ \tilde{\ell}_L^-$	$0.20^{+8.6\%}_{-19.3\%}$	$0.23^{+5.4\%+7.3\%}_{-2.6\%-9.4\%}$	$0.22^{+1.3\%+7.3\%}_{-0.3\%-9.4\%}$
	$\tilde{\ell}_R^+ \tilde{\ell}_R^-$	$0.09^{+8.5\%}_{-19.2\%}$	$0.11^{+5.4\%+8.5\%}_{-2.7\%-10.8\%}$	$0.11^{+1.2\%+8.5\%}_{-0.3\%-10.8\%}$
	$\tilde{\tau}_1^+ \tilde{\tau}_1^-$	$0.10^{+8.5\%}_{-19.2\%}$	$0.12^{+5.4\%+8.9\%}_{-2.7\%-10.6\%}$	$0.11^{+1.2\%+8.9\%}_{-0.3\%-10.6\%}$
450	$\tilde{\ell}_L^+ \tilde{\ell}_L^-$	$0.10^{+9.2\%}_{-19.9\%}$	$0.12^{+5.1\%+8.1\%}_{-3.1\%-10.2\%}$	$0.11^{+1.3\%+8.1\%}_{-0.6\%-10.2\%}$
	$\tilde{\ell}_R^+ \tilde{\ell}_R^-$	$0.05^{+9.1\%}_{-19.7\%}$	$0.06^{+5.1\%+9.9\%}_{-3.1\%-11.6\%}$	$0.06^{+1.3\%+9.9\%}_{-0.6\%-11.6\%}$
	$\tilde{\tau}_1^+ \tilde{\tau}_1^-$	$0.05^{+9.0\%}_{-19.7\%}$	$0.06^{+5.1\%+10.0\%}_{-3.1\%-11.7\%}$	$0.06^{+1.3\%+10.0\%}_{-0.6\%-11.7\%}$
500	$\tilde{\ell}_L^+ \tilde{\ell}_L^-$	$0.05^{+9.7\%}_{-20.5\%}$	$0.06^{+4.9\%+9.2\%}_{-3.3\%-10.7\%}$	$0.06^{+1.4\%+9.2\%}_{-0.9\%-10.7\%}$
	$\tilde{\ell}_R^+ \tilde{\ell}_R^-$	$0.03^{+9.6\%}_{-20.4\%}$	$0.03^{+4.9\%+11.4\%}_{-3.2\%-12.6\%}$	$0.03^{+1.4\%+11.4\%}_{-0.8\%-12.6\%}$
	$\tilde{\tau}_1^+ \tilde{\tau}_1^-$	$0.03^{+9.6\%}_{-20.3\%}$	$0.03^{+4.9\%+11.6\%}_{-3.3\%-12.7\%}$	$0.03^{+1.3\%+11.6\%}_{-0.8\%-12.7\%}$

Table 1. Total production cross sections at the LHC, running at a center-of-mass energy of 7 TeV, for first or second generation left-handed and right-handed sleptons, as well as for maximally mixing staus. Results are presented together with the associated scale and PDF uncertainties.

$M_{\tilde{\ell}}$ [GeV]	Final state	LO [fb]	NLO [fb]	NLL+NLO [fb]
50	$\tilde{\ell}_L^+ \tilde{\ell}_L^-$	$1623.00^{+7.7\%}_{-27.9\%}$	$2058.00^{+16.1\%+3.3\%}_{-1.6\%-4.4\%}$	$2039.00^{-0.8\%+3.3\%}_{-0.3\%-4.4\%}$
	$\tilde{\ell}_R^+ \tilde{\ell}_R^-$	$727.10^{+7.8\%}_{-27.8\%}$	$921.90^{+16.1\%+3.4\%}_{-1.6\%-4.5\%}$	$913.70^{-0.8\%+3.4\%}_{-0.3\%-4.5\%}$
	$\tilde{\tau}_1^+ \tilde{\tau}_1^-$	$478.40^{+6.9\%}_{-28.6\%}$	$606.70^{+16.8\%+3.9\%}_{-1.5\%-4.9\%}$	$600.10^{-0.8\%+3.9\%}_{-0.3\%-4.9\%}$
100	$\tilde{\ell}_L^+ \tilde{\ell}_L^-$	$105.50^{+0.7\%}_{-22.6\%}$	$126.50^{+16.6\%+3.7\%}_{-1.7\%-4.8\%}$	$124.80^{+0.1\%+3.7\%}_{-0.3\%-4.8\%}$
	$\tilde{\ell}_R^+ \tilde{\ell}_R^-$	$47.61^{+0.7\%}_{-22.6\%}$	$57.10^{+16.6\%+3.8\%}_{-1.7\%-5.0\%}$	$56.36^{+0.2\%+3.8\%}_{-0.3\%-5.0\%}$
	$\tilde{\tau}_1^+ \tilde{\tau}_1^-$	$48.75^{+0.7\%}_{-22.6\%}$	$58.45^{+16.6\%+3.9\%}_{-1.7\%-5.2\%}$	$57.69^{+0.2\%+3.9\%}_{-0.3\%-5.2\%}$
150	$\tilde{\ell}_L^+ \tilde{\ell}_L^-$	$23.02^{+2.6\%}_{-20.0\%}$	$27.00^{+12.6\%+4.2\%}_{-1.9\%-6.0\%}$	$26.61^{+0.5\%+4.2\%}_{-0.2\%-6.0\%}$
	$\tilde{\ell}_R^+ \tilde{\ell}_R^-$	$10.64^{+2.6\%}_{-20.0\%}$	$12.48^{+12.7\%+4.2\%}_{-1.9\%-5.7\%}$	$12.30^{+0.4\%+4.2\%}_{-0.2\%-5.7\%}$
	$\tilde{\tau}_1^+ \tilde{\tau}_1^-$	$11.20^{+2.6\%}_{-20.1\%}$	$13.14^{+12.7\%+4.4\%}_{-1.9\%-5.9\%}$	$12.96^{+0.5\%+4.4\%}_{-0.2\%-5.9\%}$
200	$\tilde{\ell}_L^+ \tilde{\ell}_L^-$	$7.30^{+4.3\%}_{-18.8\%}$	$8.47^{+10.0\%+4.9\%}_{-1.9\%-7.0\%}$	$8.35^{+0.6\%+4.9\%}_{-0.0\%-7.0\%}$
	$\tilde{\ell}_R^+ \tilde{\ell}_R^-$	$3.41^{+4.2\%}_{-18.8\%}$	$3.96^{+10.1\%+4.8\%}_{-1.9\%-6.8\%}$	$3.90^{+0.6\%+4.8\%}_{-0.1\%-6.8\%}$
	$\tilde{\tau}_1^+ \tilde{\tau}_1^-$	$3.62^{+4.2\%}_{-18.8\%}$	$4.21^{+10.1\%+4.9\%}_{-1.9\%-6.8\%}$	$4.15^{+0.6\%+4.9\%}_{-0.1\%-6.8\%}$
250	$\tilde{\ell}_L^+ \tilde{\ell}_L^-$	$2.82^{+5.4\%}_{-18.3\%}$	$3.26^{+8.3\%+5.7\%}_{-1.8\%-7.8\%}$	$3.21^{+0.7\%+5.7\%}_{-0.1\%-7.8\%}$
	$\tilde{\ell}_R^+ \tilde{\ell}_R^-$	$1.33^{+5.4\%}_{-18.3\%}$	$1.54^{+8.4\%+5.4\%}_{-1.8\%-7.6\%}$	$1.51^{+0.7\%+5.4\%}_{-0.1\%-7.6\%}$
	$\tilde{\tau}_1^+ \tilde{\tau}_1^-$	$1.42^{+5.4\%}_{-18.3\%}$	$1.64^{+8.4\%+5.6\%}_{-1.8\%-7.4\%}$	$1.61^{+0.7\%+5.6\%}_{-0.1\%-7.4\%}$
300	$\tilde{\ell}_L^+ \tilde{\ell}_L^-$	$1.24^{+6.4\%}_{-18.2\%}$	$1.43^{+7.1\%+6.3\%}_{-1.8\%-8.8\%}$	$1.40^{+0.7\%+6.3\%}_{-0.0\%-8.8\%}$
	$\tilde{\ell}_R^+ \tilde{\ell}_R^-$	$0.59^{+6.3\%}_{-18.2\%}$	$0.68^{+7.2\%+6.1\%}_{-1.8\%-8.2\%}$	$0.67^{+0.8\%+6.1\%}_{-0.0\%-8.2\%}$
	$\tilde{\tau}_1^+ \tilde{\tau}_1^-$	$0.63^{+6.3\%}_{-18.1\%}$	$0.72^{+7.2\%+6.2\%}_{-1.8\%-8.2\%}$	$0.71^{+0.7\%+6.2\%}_{-0.0\%-8.2\%}$
350	$\tilde{\ell}_L^+ \tilde{\ell}_L^-$	$0.59^{+7.1\%}_{-18.3\%}$	$0.68^{+6.3\%+7.3\%}_{-2.1\%-9.5\%}$	$0.67^{+0.9\%+7.3\%}_{-0.1\%-9.5\%}$
	$\tilde{\ell}_R^+ \tilde{\ell}_R^-$	$0.28^{+7.1\%}_{-18.2\%}$	$0.32^{+6.3\%+6.8\%}_{-2.0\%-8.9\%}$	$0.32^{+0.8\%+6.8\%}_{-0.1\%-8.9\%}$
	$\tilde{\tau}_1^+ \tilde{\tau}_1^-$	$0.30^{+7.1\%}_{-18.2\%}$	$0.35^{+6.4\%+6.8\%}_{-2.0\%-9.1\%}$	$0.34^{+0.8\%+6.8\%}_{-0.1\%-9.1\%}$
400	$\tilde{\ell}_L^+ \tilde{\ell}_L^-$	$0.30^{+7.8\%}_{-18.6\%}$	$0.35^{+5.7\%+8.3\%}_{-2.2\%-10.2\%}$	$0.34^{+1.0\%+8.3\%}_{-0.3\%-10.2\%}$
	$\tilde{\ell}_R^+ \tilde{\ell}_R^-$	$0.14^{+7.7\%}_{-18.5\%}$	$0.17^{+5.8\%+7.6\%}_{-2.0\%-9.6\%}$	$0.16^{+1.0\%+7.6\%}_{-0.2\%-9.6\%}$
	$\tilde{\tau}_1^+ \tilde{\tau}_1^-$	$0.15^{+7.7\%}_{-18.4\%}$	$0.18^{+5.8\%+7.6\%}_{-2.1\%-9.9\%}$	$0.17^{+1.0\%+7.6\%}_{-0.2\%-9.9\%}$
450	$\tilde{\ell}_L^+ \tilde{\ell}_L^-$	$0.16^{+8.4\%}_{-18.9\%}$	$0.19^{+5.3\%+9.4\%}_{-2.5\%-11.2\%}$	$0.18^{+1.2\%+9.4\%}_{-0.3\%-11.2\%}$
	$\tilde{\ell}_R^+ \tilde{\ell}_R^-$	$0.08^{+8.3\%}_{-18.8\%}$	$0.09^{+5.4\%+8.5\%}_{-2.5\%-10.5\%}$	$0.09^{+1.2\%+8.5\%}_{-0.3\%-10.5\%}$
	$\tilde{\tau}_1^+ \tilde{\tau}_1^-$	$0.08^{+8.3\%}_{-18.8\%}$	$0.10^{+5.4\%+8.6\%}_{-2.5\%-10.6\%}$	$0.09^{+1.2\%+8.6\%}_{-0.3\%-10.6\%}$
500	$\tilde{\ell}_L^+ \tilde{\ell}_L^-$	$0.09^{+8.9\%}_{-19.4\%}$	$0.10^{+5.1\%+10.8\%}_{-2.5\%-11.9\%}$	$0.10^{+1.3\%+10.8\%}_{-0.6\%-11.9\%}$
	$\tilde{\ell}_R^+ \tilde{\ell}_R^-$	$0.04^{+8.8\%}_{-19.3\%}$	$0.05^{+5.1\%+9.6\%}_{-2.7\%-11.3\%}$	$0.05^{+1.3\%+9.6\%}_{-0.5\%-11.3\%}$
	$\tilde{\tau}_1^+ \tilde{\tau}_1^-$	$0.05^{+8.8\%}_{-19.3\%}$	$0.05^{+5.1\%+9.7\%}_{-2.8\%-11.4\%}$	$0.05^{+1.3\%+9.7\%}_{-0.5\%-11.4\%}$

Table 2. Same as Table 1, but for a center-of-mass energy of 8 TeV.

generated events are reweighted according to the NLL+NLO predictions as computed by RESUMMINO [39]. Event analysis is finally performed by means of the MADANALYSIS 5 program [75, 76], after having reconstructed the jets with the anti- k_T algorithm (using a radius parameter set to $R = 0.5$) [77] as implemented in the FASTJET package [78].

By the time this work was being completed, additional simplified models with different slepton/neutralino definitions have been investigated by both the ATLAS and CMS collaborations [11, 16], extending the earlier analyses of Refs. [7, 15]. When a comparison is possible, the obtained results have been found to fairly agree with our predictions.

4.1 Revisiting ATLAS searches for first and second generation sleptons

In this section, we start by recasting the ATLAS analysis of Ref. [7] dedicated to first and second generation slepton searches in LHC collisions at a center-of-mass energy of 7 TeV. After generating signal events by means of the above-mentioned simulation setup, we apply the selection strategy designed by the ATLAS collaboration and demand the following criteria to be satisfied.

- We require the event final state to contain exactly two isolated leptons of the same flavor, their transverse momentum being imposed to be greater than 10 GeV and their pseudorapidity to fulfill $|\eta| \leq 2.47$ and $|\eta| \leq 2.4$ for electrons and muons, respectively. The isolation is enforced by constraining the transverse activity in a cone of radius $R = \sqrt{\Delta\varphi^2 + \Delta\eta^2} = 0.2$ centered on the lepton, φ being the azimuthal angle with respect to the beam direction, to be less than 10% of the lepton p_T for electrons and less than 1.8 GeV for muons.
- Events featuring at least one jet with a transverse momentum $p_T \geq 30$ GeV and a pseudorapidity $|\eta| \leq 2.5$ are vetoed.
- The lepton pair is asked not to be compatible with a Z -boson, the dilepton invariant mass $m_{\ell\ell}$ being constrained to be off the Z -boson peak, $m_{\ell\ell} \notin [80, 100]$ GeV.
- We ask the final state to contain a significant quantity of relative missing transverse energy $\cancel{E}_T^{\text{rel}} \geq 40$ GeV, where the relative missing transverse energy is defined as the missing transverse energy \cancel{E}_T when the azimuthal angle $\tilde{\varphi}$ between the direction of the missing momentum and that of the nearest reconstructed object is larger than $\pi/2$, and by $\cancel{E}_T^{\text{rel}} = \cancel{E}_T \sin \tilde{\varphi}$ otherwise.
- The properties of the m_{T2} variable [79] are finally exploited and we select events for which $m_{T2} \geq 90$ GeV.

Focusing on different scenarios from the class of simplified models introduced in Section 2.1, the results are presented in Figure 6. We first restrict ourselves to the production of a pair of left-handed selectrons decaying into a pair of leptons and missing energy. We consider three choices for the nature of the lightest neutralino, namely a pure bino state ($N_1 = 1$; $N_2 = N_3 = N_4 = 0$; left panel of the figure), a pure wino state ($N_2 = 1$; $N_1 = N_3 = N_4 = 0$; central panel of the figure) and a mixed state ($N_1 = N_2 = 1/\sqrt{2}$;

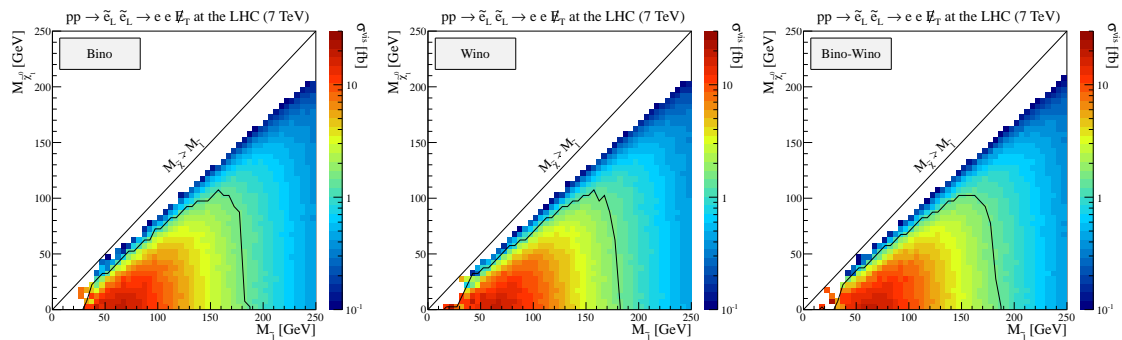


Figure 6. 95% confidence exclusion limit for left-handed selectron pair production, given in the $(M_{\tilde{\ell}}, M_{\tilde{\chi}_1^0})$ mass plane of the simplified model of Section 2.1 for different choices of the neutralino nature taken as bino (left), wino (center) and mixed (right). We present the visible cross section after applying the ATLAS selection strategy depicted in the text. The limits are extracted for 4.7 fb^{-1} of LHC collisions at a center-of-mass energy of 7 TeV.

$N_3 = N_4 = 0$; right panel of the figure). We show the visible cross section σ^{vis} for a center-of-mass energy of 7 TeV, defined as the fraction of the cross section giving rise to events that can be observed by the ATLAS experiment when using the analysis described above, in $(M_{\tilde{\ell}}, M_{\tilde{\chi}_1^0})$ mass planes. In addition, we superimpose to the cross section results the 95% confidence level contours that can be extracted from the ATLAS bounds on the visible cross section $\sigma^{\text{vis}} \leq 1.5 \text{ fb}$.

The selectron being a scalar field, we expect the direct production of a pair of selectrons followed by their decay into electrons and lightest neutralinos to be non-sensitive to the neutralino nature. This is illustrated by the three panels of Figure 6, that show that the LHC reach is independent of the neutralino nature. For almost massless neutralinos, selectrons with masses ranging up to about 175 GeV are found excluded by 4.7 fb^{-1} of 7 TeV LHC data. This upper bound holds for any neutralino mass smaller than 100 GeV, a value from which the sensitivity drops so that no constraints can be derived from data. In addition, benchmark models featuring a compressed spectrum still offer a way to evade LHC constraints since final state leptons originating from slepton decays are in this case too soft for being detected.

This independence of the results on the neutralino nature is also depicted on Figure 7, where we present different kinematical observables. We focus on the transverse-momentum spectra of the two detected leptons ℓ_1 and ℓ_2 (first line of the figure), the missing transverse energy distribution (left panel of the second line of the figure), the transverse mass of the lepton pair $M_T(\ell_1\ell_2)$ (right panel of the second line of the figure), the angular distance in the azimuthal plane between the two leptons $\Delta\Phi(\ell_1\ell_2)$ (left panel of the third line of the figure), their pseudorapidity separation $\Delta\eta(\ell_1\ell_2)$ (right panel of the third line of the figure), the angular distance in the azimuthal plane of the missing momentum with the lepton pair $\Delta\Phi(\ell_1\ell_2, \cancel{E}_T)$ as well as the one with the hardest lepton $\Delta\Phi(\ell_1, \cancel{E}_T)$ (last line of the figure). On the different subfigures, we superimpose results obtained for simplified models exhibiting different neutralino natures and fix, for the sake of the example, the

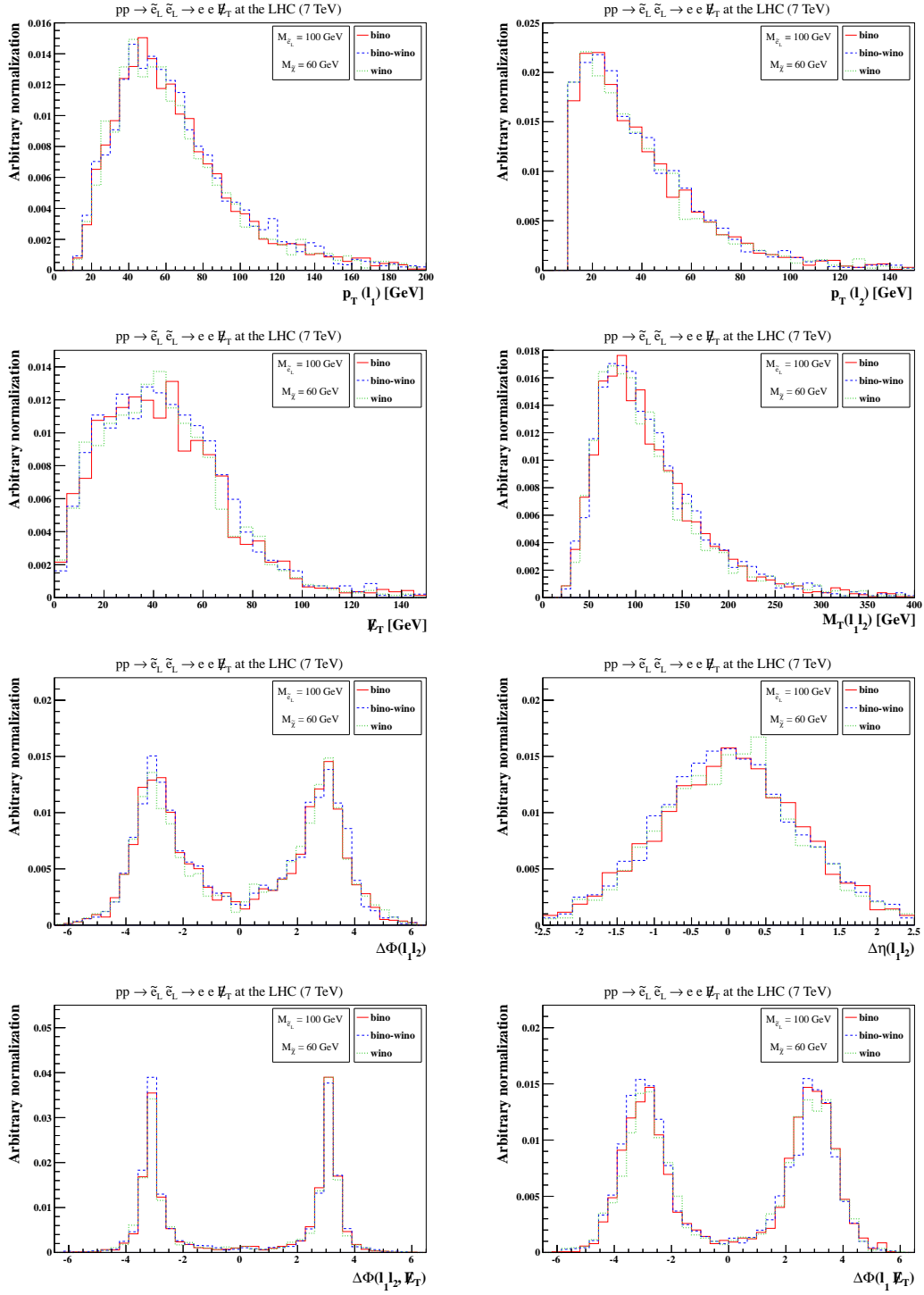


Figure 7. Properties of the dilepton plus missing energy final state arising from the production and decay of a pair of left-handed selectrons, for a benchmark scenario where the neutralino mass is set to 60 GeV and the left-handed selectron mass to 100 GeV. The distributions are shown for different choices of the neutralino nature.

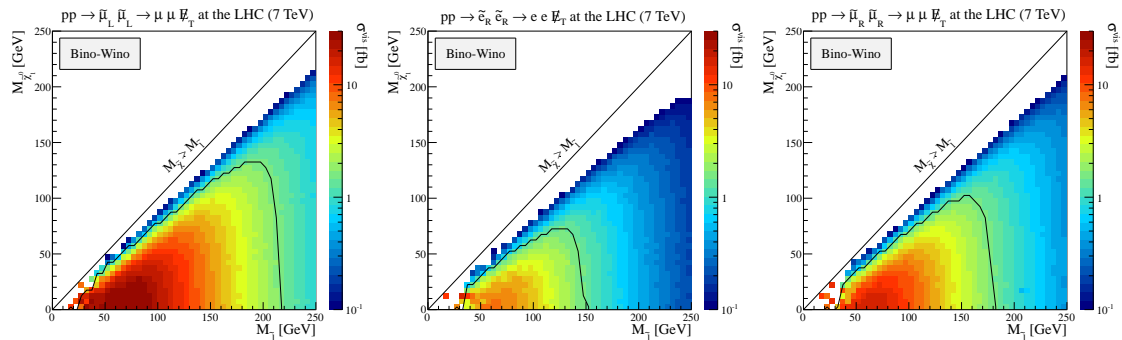


Figure 8. Same as in Figure 6, but for the production of a pair of left-handed smuons (left), right-handed selectrons (center) and right-handed smuons (right).

slepton and neutralino masses to 100 GeV and 60 GeV, respectively. From now on, we consider the neutralino to be a mixed wino-bino state.

In Figure 8, we study the dependence of the results on the left-handed and right-handed nature of the produced sleptons, as well as on their flavor. Concerning muonic final states, visible cross sections larger than 1.6 fb have been excluded by the ATLAS collaboration. The resulting 95% exclusion limits are presented on the left and right panels of the figure for left-handed and right-handed muons, respectively. The central panel of the figure is dedicated to the only species of sleptons not considered yet, *i.e.*, right-handed selectrons. The different selections of muon and electron candidates, together with the slightly different detector acceptance for both types of particles, imply that the ATLAS results of Ref. [7] more strongly constrain the simplified model parameter space related to smuon models than the one related to selectron models. In addition, the larger left-handed slepton production rate allows to reach a larger mass range as when considering right-handed sleptons. Consequently, masses ranging up to 175 GeV (220 GeV) and 150 GeV (180 GeV) are found excluded for models containing a left-handed and right-handed selectrons (smuons), respectively, when the neutralino is assumed massless. Contrary, when the neutralino is heavier than 100 GeV and 60 GeV in the left-handed and right-handed selectron cases, and heavier than 130 GeV and 100 GeV in the left-handed and right-handed smuon cases, respectively, all sensitivity is lost. These properties are also illustrated on Figure 9 where we present the variations of the kinematical distributions already considered in Figure 7, but this time when we modify the nature of the produced sleptons. We compare the shapes of the various distributions and observe differences for electron and muon spectra, the figures having been obtained prior the Z -boson veto, missing energy selection and the m_{T2} selection steps of the analysis.

4.2 Revisiting CMS searches for first and second generation sleptons

First and second generation sleptons have also been searched for in LHC collisions at a center-of-mass energy of 8 TeV, for instance in the CMS analysis of Ref. [15] which we focus on in this subsection. This analysis contains several signal regions, one of them being expected to be sensitive to direct slepton pair production followed by their decays into

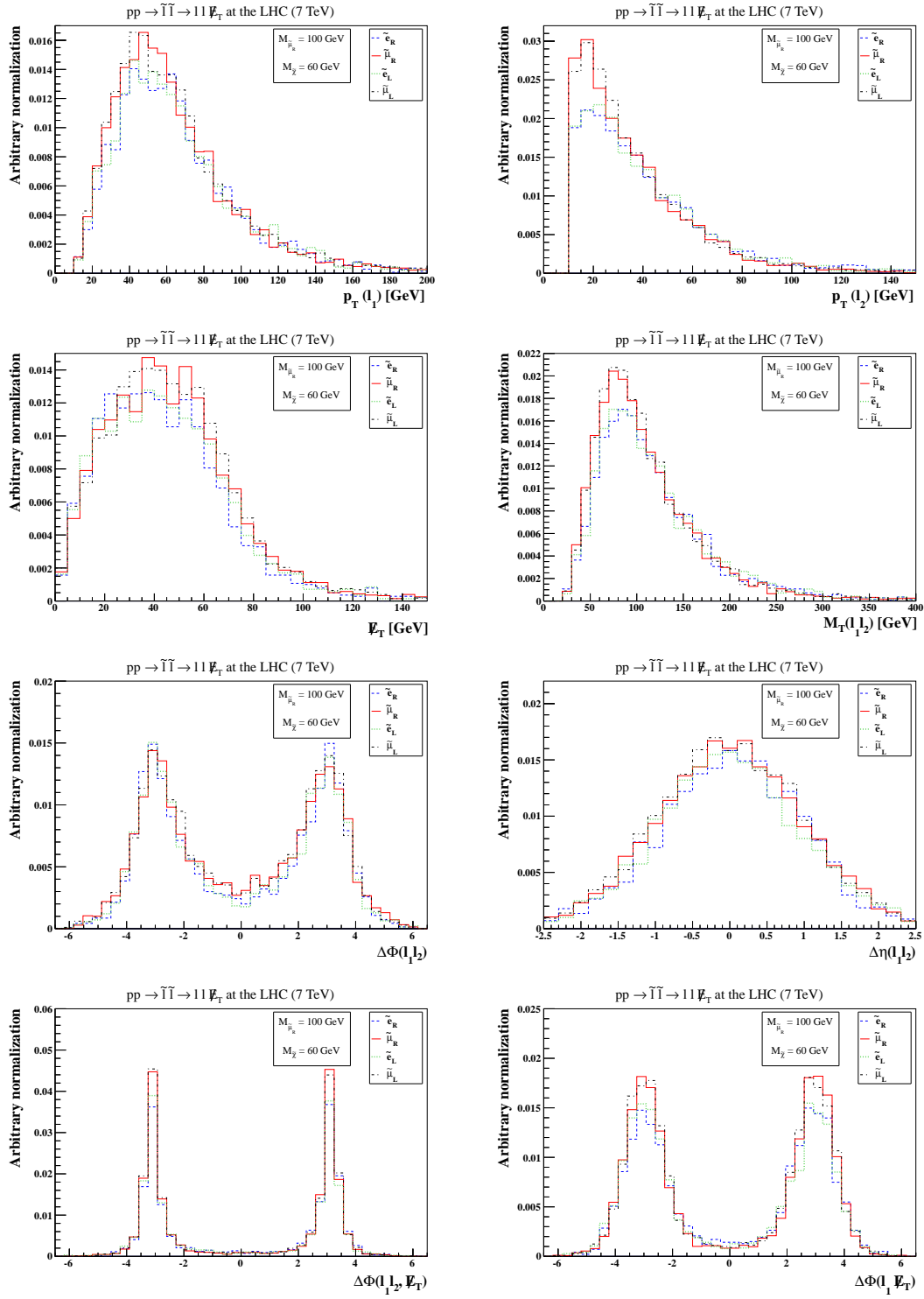


Figure 9. Same as in Figure 7 but when the neutralino nature is fixed to a bino-wino mixed state and for the production of different types of sleptons.

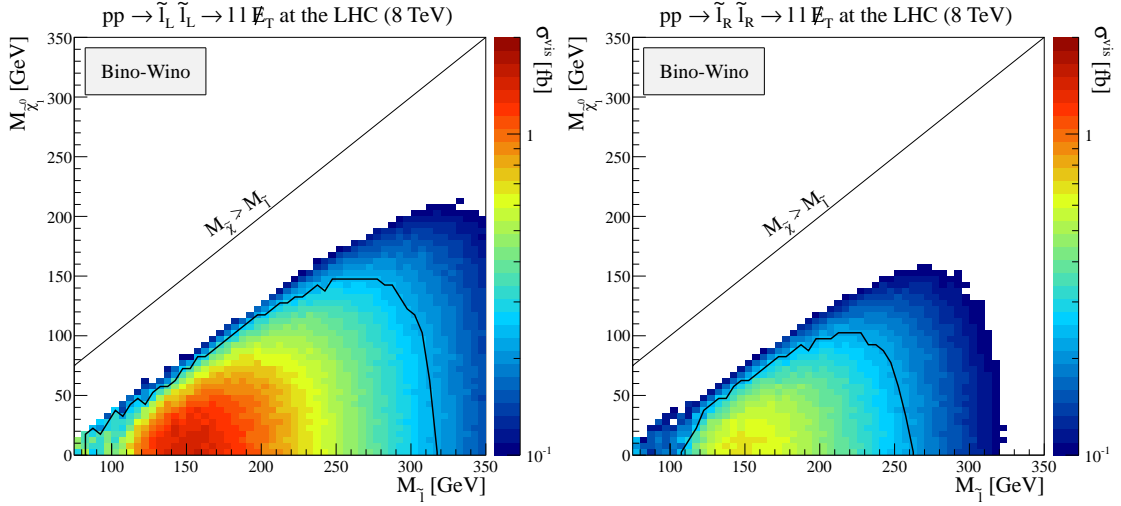


Figure 10. 95% confidence exclusion limit for left-handed (left) and right-handed (right) slepton pair production, given in the $(M_{\tilde{\ell}}, M_{\tilde{\chi}^0})$ mass plane of the simplified model of Section 2.1, for a mixed bino-wino neutralino and after summing over both first and second slepton generations. We present signal cross sections σ^{vis} that are visible after having applied the CMS selection strategy depicted in the text. The limits are extracted for 9.2 fb^{-1} of LHC collisions at a center-of-mass energy of 8 TeV.

the associated Standard Model partners and missing energy. The corresponding selection strategy is defined as follows.

- We select jets whose transverse momentum is larger than 30 GeV and pseudorapidity $|\eta| \leq 2.5$. A veto on events containing at least one b -tagged jet is then applied, our b -tagging efficiency and mistagging rates being described in Ref. [68].
- Signal electrons (muons) are defined as isolated electron (muon) candidates with a transverse momentum larger than 20 GeV and a pseudorapidity such that $|\eta| \leq 2.4$. The isolation criterion is imposed by requiring that the activity in a cone of radius $R = 0.3$ around the lepton is smaller than 15% of the lepton p_T .
- We select events containing two leptons of the same flavor and with an opposite electric charge and impose the dilepton invariant mass $m_{\ell\ell}$ to be first larger than 12 GeV (to veto events with a leptonically-decaying hadronic resonance) and next not compatible with the mass of the Z -boson, $m_{\ell\ell} \notin [75, 105] \text{ GeV}$.
- Each jet lying within a cone of radius $R = 0.4$ around an electron is removed from the analysis.
- We require the event final state to feature at least 60 GeV of missing transverse energy and a transverse contranverse mass $M_{CT\perp}$ [80] larger than 100 GeV.

We reinterpret this analysis in the framework of the pair production of left-handed and right-handed sleptons in the left and right panels of Figure 10, respectively. Those results

are extracted after summing over both selectron and smuon channels, considering the two types of superpartners mass-degenerate, and our predictions are given for an integrated luminosity of 9.2 fb^{-1} of LHC collisions at a center-of-mass energy of 8 TeV. We present, in both panels of the figure, $(M_{\tilde{\ell}}, M_{\tilde{\chi}_1^0})$ planes with the visible cross section defined as the fraction of the cross section remaining after applying the CMS selection described above. We then superimpose 95% confidence level exclusion contours extracted from the observation by the CMS experiment of six data events. This number is compared to our computations of the signal contribution, summed to the Standard Model expectation as calculated by the CMS experiment, which is given by 14.2 ± 4.5 events.

We observe that left-handed and right-handed sleptons of masses ranging up to 310 GeV and 250 GeV are excluded, respectively, in the case the lightest neutralino is massless. These upper bounds hold, like for the results shown in Section 4.1, for heavier neutralinos with masses smaller than 150 GeV (100 GeV) in the case of left-handed (right-handed) sleptons. Moreover, the CMS analysis is found to be insensitive to sleptons via their direct production mechanism both when the neutralino mass is larger than those values, and when the mass difference $M_{\tilde{\ell}} - M_{\tilde{\chi}_1^0}$ becomes smaller than 70 GeV, the bulk of the Standard Model leptons originating from the slepton decays being soft enough not to populate the signal region.

5 Conclusion

In conclusion, we have updated in this paper our precision predictions at next-to-leading order of perturbative QCD matched to resummation at the next-to-leading logarithmic accuracy for direct slepton pair production in proton-proton collisions. We used simplified models, which are now commonly adopted by the experimental collaborations for selectrons and smuons as well as mixing staus, as benchmarks for total cross sections at past ($\sqrt{S} = 7 \text{ TeV}$ and 8 TeV) and future ($\sqrt{S} = 13 \text{ TeV}$ and 14 TeV) center-of-mass energies. Our calculations stabilized the cross sections considerably with respect to renormalization and factorization scale uncertainties, but also with respect to parton density variations. The most precise slepton-pair production cross section values have in this way been made available so that they can now be used in all future LHC experimental analyses dedicated to the direct search for sleptons.

They were then employed in combination with modern Monte Carlo techniques to reanalyze recent ATLAS and CMS slepton searches for various assumptions on the decomposition of the sleptons and their neutralino decay products, giving rise to more precise and more specific current exclusion limits for first- and second-generation sleptons. We conclude from our results that exhibit different limits for selectron and smuon scenarios and for both chiralities, that it might be valuable to present, in the future, slepton results without combining left-handed and right-handed channels, as well as selectron and smuon ones. However, a reanalysis of an ATLAS stau search within our simplified model parameter space proved to be impossible due to a complicated tau reconstruction together with small signal cross sections, in particular once tau decay branching ratios were included.

A Total cross sections at center-of-mass energies of 13 TeV and 14 TeV

This appendix complements the summary tables of Section 3.4 and contains total cross sections for slepton pair production at the LHC. We focus on the future runs at center-of-mass energies of 13 TeV and 14 TeV and respectively present the results, in Table 3 and Table 4, for specific choices of the slepton mass. Our predictions are given together with the uncertainties arising from the variation of the unphysical scales by a factor of two around their central value chosen to be the produced slepton mass, as well as those issued from the choice of the parton densities. The latter have been computed by using the 52 parton density fits obtained from variations along the 26 eigenvectors of the covariance matrix associated with the CT10 NLO best fit of the CTEQ collaboration, adopted as our central choice.

Acknowledgments

This work has been supported by the BMBF Theorie-Verbund and by the Theory-LHC-France initiative of the CNRS/IN2P3.

References

- [1] **ATLAS Collaboration**, G. Aad et al., *Observation of a new particle in the search for the Standard Model Higgs boson with the ATLAS detector at the LHC*, *Phys.Lett.* **B716** (2012) 1–29, [[arXiv:1207.7214](#)].
- [2] **CMS Collaboration**, S. Chatrchyan et al., *Observation of a new boson at a mass of 125 GeV with the CMS experiment at the LHC*, *Phys.Lett.* **B716** (2012) 30–61, [[arXiv:1207.7235](#)].
- [3] H. P. Nilles, *Supersymmetry, Supergravity and Particle Physics*, *Phys.Rept.* **110** (1984) 1–162.
- [4] H. E. Haber and G. L. Kane, *The Search for Supersymmetry: Probing Physics Beyond the Standard Model*, *Phys.Rept.* **117** (1985) 75–263.
- [5] <https://twiki.cern.ch/twiki/bin/view/AtlasPublic>.
- [6] <https://twiki.cern.ch/twiki/bin/view/CMSPublic/PhysicsResults>.
- [7] **ATLAS Collaboration**, G. Aad et al., *Search for direct slepton and gaugino production in final states with two leptons and missing transverse momentum with the ATLAS detector in pp collisions at $\sqrt{s} = 7$ TeV*, *Phys.Lett.* **B718** (2013) 879–901, [[arXiv:1208.2884](#)].
- [8] **ATLAS Collaboration**, G. Aad et al., *Search for direct production of charginos and neutralinos in events with three leptons and missing transverse momentum in $\sqrt{s} = 7$ TeV pp collisions with the ATLAS detector*, *Phys.Lett.* **B718** (2013) 841–859, [[arXiv:1208.3144](#)].
- [9] **ATLAS Collaboration**, G. Aad et al., *Search for supersymmetry in events with three leptons and missing transverse momentum in $\sqrt{s} = 7$ TeV pp collisions with the ATLAS detector*, *Phys.Rev.Lett.* **108** (2012) 261804, [[arXiv:1204.5638](#)].
- [10] **ATLAS Collaboration**, *Search for electroweak production of supersymmetric particles in final states with at least two hadronically decaying taus and missing transverse momentum with the ATLAS detector in proton-proton collisions at $\sqrt{s} = 8$ TeV*, .

$M_{\tilde{\ell}}$ [GeV]	Final state	LO [fb]	NLO [fb]	NLO+NLL [fb]
50	$\tilde{\ell}_L^+ \tilde{\ell}_L^-$	$3194.60^{+9.8\%}_{-11.2\%}$	$4139.50^{+1.2\%+3.1\%}_{-0.7\%-3.7\%}$	$4104.90^{+1.4\%+3.1\%}_{-1.6\%-3.6\%}$
	$\tilde{\ell}_R^+ \tilde{\ell}_R^-$	$1071.70^{+9.8\%}_{-11.1\%}$	$1389.10^{+1.1\%+3.2\%}_{-0.8\%-3.8\%}$	$1377.60^{+1.4\%+3.3\%}_{-1.6\%-3.7\%}$
	$\tilde{\tau}_1^+ \tilde{\tau}_1^-$	$731.01^{+8.8\%}_{-10.2\%}$	$952.84^{+0.7\%+3.8\%}_{-0.2\%-4.5\%}$	$943.29^{+1.2\%+3.8\%}_{-1.3\%-4.4\%}$
100	$\tilde{\ell}_L^+ \tilde{\ell}_L^-$	$223.80^{+2.9\%}_{-3.9\%}$	$273.89^{+1.5\%+3.2\%}_{-0.8\%-3.5\%}$	$270.79^{+0.0\%+3.3\%}_{-0.4\%-3.4\%}$
	$\tilde{\ell}_R^+ \tilde{\ell}_R^-$	$79.68^{+2.9\%}_{-3.9\%}$	$97.59^{+1.5\%+3.5\%}_{-0.8\%-4.1\%}$	$96.51^{+0.0\%+3.6\%}_{-0.3\%-4.0\%}$
	$\tilde{\tau}_1^+ \tilde{\tau}_1^-$	$84.85^{+2.9\%}_{-3.9\%}$	$103.94^{+1.5\%+3.7\%}_{-0.9\%-4.3\%}$	$102.77^{+0.0\%+3.7\%}_{-0.3\%-4.3\%}$
150	$\tilde{\ell}_L^+ \tilde{\ell}_L^-$	$53.88^{+0.1\%}_{-0.7\%}$	$64.12^{+1.9\%+3.4\%}_{-1.3\%-3.9\%}$	$63.34^{+0.1\%+3.4\%}_{-0.3\%-3.9\%}$
	$\tilde{\ell}_R^+ \tilde{\ell}_R^-$	$19.81^{+0.1\%}_{-0.7\%}$	$23.60^{+1.9\%+3.7\%}_{-1.3\%-4.4\%}$	$23.32^{+0.1\%+3.7\%}_{-0.3\%-4.5\%}$
	$\tilde{\tau}_1^+ \tilde{\tau}_1^-$	$21.69^{+0.1\%}_{-0.7\%}$	$25.83^{+1.9\%+3.7\%}_{-1.3\%-4.6\%}$	$25.53^{+0.1\%+3.8\%}_{-0.3\%-4.6\%}$
200	$\tilde{\ell}_L^+ \tilde{\ell}_L^-$	$18.84^{+1.3\%}_{-1.6\%}$	$22.07^{+2.0\%+3.6\%}_{-1.5\%-4.4\%}$	$21.81^{+0.1\%+3.6\%}_{-0.4\%-4.4\%}$
	$\tilde{\ell}_R^+ \tilde{\ell}_R^-$	$7.03^{+1.3\%}_{-1.6\%}$	$8.25^{+2.0\%+3.9\%}_{-1.5\%-4.9\%}$	$8.15^{+0.1\%+3.9\%}_{-0.4\%-4.9\%}$
	$\tilde{\tau}_1^+ \tilde{\tau}_1^-$	$7.77^{+1.3\%}_{-1.6\%}$	$9.11^{+2.0\%+3.9\%}_{-1.5\%-5.0\%}$	$9.00^{+0.1\%+3.9\%}_{-0.4\%-5.0\%}$
250	$\tilde{\ell}_L^+ \tilde{\ell}_L^-$	$8.04^{+2.8\%}_{-2.9\%}$	$9.33^{+2.0\%+3.9\%}_{-1.7\%-4.9\%}$	$9.21^{+0.3\%+3.9\%}_{-0.4\%-5.0\%}$
	$\tilde{\ell}_R^+ \tilde{\ell}_R^-$	$3.03^{+2.8\%}_{-2.8\%}$	$3.52^{+2.0\%+4.2\%}_{-1.7\%-5.3\%}$	$3.47^{+0.2\%+4.2\%}_{-0.4\%-5.3\%}$
	$\tilde{\tau}_1^+ \tilde{\tau}_1^-$	$3.36^{+2.8\%}_{-2.8\%}$	$3.90^{+2.0\%+4.2\%}_{-1.7\%-5.4\%}$	$3.85^{+0.1\%+4.3\%}_{-0.4\%-5.4\%}$
300	$\tilde{\ell}_L^+ \tilde{\ell}_L^-$	$3.89^{+4.0\%}_{-3.8\%}$	$4.49^{+2.0\%+4.2\%}_{-1.8\%-5.4\%}$	$4.43^{+0.1\%+4.2\%}_{-0.3\%-5.4\%}$
	$\tilde{\ell}_R^+ \tilde{\ell}_R^-$	$1.48^{+3.9\%}_{-3.8\%}$	$1.70^{+2.0\%+4.5\%}_{-1.8\%-5.7\%}$	$1.68^{+0.2\%+4.5\%}_{-0.3\%-5.7\%}$
	$\tilde{\tau}_1^+ \tilde{\tau}_1^-$	$1.64^{+3.9\%}_{-3.8\%}$	$1.89^{+2.0\%+4.6\%}_{-1.8\%-5.8\%}$	$1.87^{+0.2\%+4.6\%}_{-0.3\%-5.8\%}$
350	$\tilde{\ell}_L^+ \tilde{\ell}_L^-$	$2.05^{+4.9\%}_{-4.6\%}$	$2.36^{+2.1\%+4.6\%}_{-2.0\%-5.9\%}$	$2.33^{+0.0\%+4.6\%}_{-0.3\%-5.9\%}$
	$\tilde{\ell}_R^+ \tilde{\ell}_R^-$	$0.78^{+4.8\%}_{-4.5\%}$	$0.90^{+2.1\%+4.9\%}_{-2.0\%-6.1\%}$	$0.89^{+0.0\%+4.9\%}_{-0.3\%-6.1\%}$
	$\tilde{\tau}_1^+ \tilde{\tau}_1^-$	$0.87^{+4.8\%}_{-4.5\%}$	$1.00^{+2.0\%+5.0\%}_{-2.0\%-6.2\%}$	$0.99^{+0.0\%+4.9\%}_{-0.3\%-6.3\%}$
400	$\tilde{\ell}_L^+ \tilde{\ell}_L^-$	$1.15^{+5.7\%}_{-5.2\%}$	$1.32^{+2.1\%+5.0\%}_{-2.1\%-6.3\%}$	$1.31^{+0.0\%+5.0\%}_{-0.3\%-6.5\%}$
	$\tilde{\ell}_R^+ \tilde{\ell}_R^-$	$0.44^{+5.7\%}_{-5.2\%}$	$0.51^{+2.1\%+5.3\%}_{-2.1\%-6.6\%}$	$0.50^{+0.0\%+5.2\%}_{-0.4\%-6.7\%}$
	$\tilde{\tau}_1^+ \tilde{\tau}_1^-$	$0.49^{+5.6\%}_{-5.2\%}$	$0.56^{+2.1\%+5.4\%}_{-2.1\%-6.6\%}$	$0.56^{+0.0\%+5.3\%}_{-0.3\%-6.8\%}$
450	$\tilde{\ell}_L^+ \tilde{\ell}_L^-$	$0.68^{+6.4\%}_{-5.8\%}$	$0.78^{+2.1\%+5.4\%}_{-2.2\%-6.8\%}$	$0.77^{+0.0\%+5.4\%}_{-0.3\%-6.8\%}$
	$\tilde{\ell}_R^+ \tilde{\ell}_R^-$	$0.26^{+6.4\%}_{-5.7\%}$	$0.30^{+2.1\%+5.7\%}_{-2.2\%-7.0\%}$	$0.30^{+0.0\%+5.7\%}_{-0.3\%-7.0\%}$
	$\tilde{\tau}_1^+ \tilde{\tau}_1^-$	$0.29^{+6.3\%}_{-5.7\%}$	$0.33^{+2.1\%+5.8\%}_{-2.2\%-7.0\%}$	$0.33^{+0.0\%+5.7\%}_{-0.3\%-7.1\%}$
500	$\tilde{\ell}_L^+ \tilde{\ell}_L^-$	$0.42^{+7.1\%}_{-6.3\%}$	$0.48^{+2.1\%+5.8\%}_{-2.3\%-7.2\%}$	$0.47^{+0.0\%+5.9\%}_{-0.4\%-7.1\%}$
	$\tilde{\ell}_R^+ \tilde{\ell}_R^-$	$0.16^{+7.0\%}_{-6.2\%}$	$0.18^{+2.1\%+6.1\%}_{-2.3\%-7.4\%}$	$0.18^{+0.0\%+6.2\%}_{-0.3\%-7.4\%}$
	$\tilde{\tau}_1^+ \tilde{\tau}_1^-$	$0.18^{+7.0\%}_{-6.2\%}$	$0.21^{+2.1\%+6.2\%}_{-2.3\%-7.5\%}$	$0.20^{+0.0\%+6.3\%}_{-0.3\%-7.4\%}$

Table 3. Total production cross sections at the LHC, running at a center-of-mass energy of 13 TeV, for first or second generation left-handed and right-handed sleptons, as well as for maximally mixing staus. Results are presented together with the associated scale and PDF uncertainties.

$M_{\tilde{\ell}}$ [GeV]	Final state	LO [fb]	NLO [fb]	NLO+NLL [fb]
50	$\tilde{\ell}_L^+ \tilde{\ell}_L^-$	$3467.30^{+10.3\%}_{-11.7\%}$	$4507.50^{+1.3\%+3.1\%}_{-0.9\%-3.8\%}$	$4470.80^{+1.6\%+3.2\%}_{-1.6\%-3.7\%}$
	$\tilde{\ell}_R^+ \tilde{\ell}_R^-$	$1162.40^{+10.3\%}_{-11.6\%}$	$1511.40^{+1.3\%+3.2\%}_{-1.0\%-3.8\%}$	$1499.50^{+1.6\%+3.2\%}_{-1.7\%-3.8\%}$
	$\tilde{\tau}_1^+ \tilde{\tau}_1^-$	$792.71^{+9.3\%}_{-10.7\%}$	$1037.10^{+0.9\%+3.8\%}_{-0.4\%-4.5\%}$	$1027.10^{+1.3\%+3.8\%}_{-1.4\%-4.4\%}$
100	$\tilde{\ell}_L^+ \tilde{\ell}_L^-$	$246.85^{+3.4\%}_{-4.4\%}$	$303.04^{+1.3\%+3.2\%}_{-0.7\%-3.4\%}$	$299.78^{+0.0\%+3.2\%}_{-0.5\%-3.4\%}$
	$\tilde{\ell}_R^+ \tilde{\ell}_R^-$	$87.75^{+3.3\%}_{-4.4\%}$	$107.81^{+1.4\%+3.5\%}_{-0.7\%-4.0\%}$	$106.68^{+0.0\%+3.5\%}_{-0.4\%-4.1\%}$
	$\tilde{\tau}_1^+ \tilde{\tau}_1^-$	$93.41^{+3.3\%}_{-4.3\%}$	$114.79^{+1.4\%+3.6\%}_{-0.7\%-4.3\%}$	$113.58^{+0.0\%+3.6\%}_{-0.4\%-4.3\%}$
150	$\tilde{\ell}_L^+ \tilde{\ell}_L^-$	$60.19^{+0.5\%}_{-1.2\%}$	$71.82^{+1.8\%+3.3\%}_{-1.2\%-3.8\%}$	$70.98^{+0.0\%+3.3\%}_{-0.3\%-3.8\%}$
	$\tilde{\ell}_R^+ \tilde{\ell}_R^-$	$22.09^{+0.5\%}_{-1.2\%}$	$26.38^{+1.8\%+3.6\%}_{-1.2\%-4.3\%}$	$26.09^{+0.0\%+3.6\%}_{-0.4\%-4.3\%}$
	$\tilde{\tau}_1^+ \tilde{\tau}_1^-$	$24.18^{+0.5\%}_{-1.2\%}$	$28.88^{+1.8\%+3.7\%}_{-1.2\%-4.5\%}$	$28.55^{+0.0\%+3.7\%}_{-0.4\%-4.5\%}$
200	$\tilde{\ell}_L^+ \tilde{\ell}_L^-$	$21.29^{+0.9\%}_{-1.2\%}$	$25.00^{+1.9\%+3.5\%}_{-1.4\%-4.2\%}$	$24.70^{+0.1\%+3.5\%}_{-0.4\%-4.3\%}$
	$\tilde{\ell}_R^+ \tilde{\ell}_R^-$	$7.94^{+0.8\%}_{-1.2\%}$	$9.32^{+1.9\%+3.8\%}_{-1.4\%-4.7\%}$	$9.22^{+0.1\%+3.8\%}_{-0.4\%-4.8\%}$
	$\tilde{\tau}_1^+ \tilde{\tau}_1^-$	$8.76^{+0.8\%}_{-1.2\%}$	$10.29^{+1.9\%+3.9\%}_{-1.4\%-4.9\%}$	$10.17^{+0.1\%+3.9\%}_{-0.4\%-4.9\%}$
250	$\tilde{\ell}_L^+ \tilde{\ell}_L^-$	$9.19^{+2.4\%}_{-2.5\%}$	$10.69^{+2.0\%+3.8\%}_{-1.6\%-4.7\%}$	$10.55^{+0.0\%+3.8\%}_{-0.3\%-4.8\%}$
	$\tilde{\ell}_R^+ \tilde{\ell}_R^-$	$3.46^{+2.3\%}_{-2.4\%}$	$4.02^{+2.0\%+4.0\%}_{-1.6\%-5.2\%}$	$3.97^{+0.0\%+4.1\%}_{-0.4\%-5.2\%}$
	$\tilde{\tau}_1^+ \tilde{\tau}_1^-$	$3.83^{+2.3\%}_{-2.4\%}$	$4.46^{+2.0\%+4.1\%}_{-1.6\%-5.2\%}$	$4.41^{+0.0\%+4.1\%}_{-0.4\%-5.3\%}$
300	$\tilde{\ell}_L^+ \tilde{\ell}_L^-$	$4.50^{+3.5\%}_{-3.4\%}$	$5.20^{+2.0\%+4.1\%}_{-1.7\%-5.2\%}$	$5.13^{+0.2\%+4.1\%}_{-0.4\%-5.3\%}$
	$\tilde{\ell}_R^+ \tilde{\ell}_R^-$	$1.70^{+3.5\%}_{-3.4\%}$	$1.97^{+2.0\%+4.3\%}_{-1.7\%-5.5\%}$	$1.94^{+0.2\%+4.4\%}_{-0.4\%-5.6\%}$
	$\tilde{\tau}_1^+ \tilde{\tau}_1^-$	$1.89^{+3.4\%}_{-3.4\%}$	$2.19^{+2.0\%+4.4\%}_{-1.7\%-5.6\%}$	$2.16^{+0.2\%+4.4\%}_{-0.4\%-5.7\%}$
350	$\tilde{\ell}_L^+ \tilde{\ell}_L^-$	$2.40^{+4.5\%}_{-4.2\%}$	$2.76^{+2.0\%+4.4\%}_{-1.9\%-5.6\%}$	$2.73^{+0.0\%+4.3\%}_{-0.3\%-5.8\%}$
	$\tilde{\ell}_R^+ \tilde{\ell}_R^-$	$0.91^{+4.4\%}_{-4.1\%}$	$1.05^{+2.0\%+4.7\%}_{-1.9\%-5.9\%}$	$1.04^{+0.0\%+4.7\%}_{-0.3\%-6.1\%}$
	$\tilde{\tau}_1^+ \tilde{\tau}_1^-$	$1.02^{+4.4\%}_{-4.1\%}$	$1.17^{+2.0\%+4.8\%}_{-1.9\%-6.0\%}$	$1.16^{+0.1\%+4.8\%}_{-0.3\%-6.0\%}$
400	$\tilde{\ell}_L^+ \tilde{\ell}_L^-$	$1.36^{+5.3\%}_{-4.9\%}$	$1.56^{+2.0\%+4.8\%}_{-2.0\%-6.1\%}$	$1.54^{+0.0\%+4.9\%}_{-0.3\%-6.1\%}$
	$\tilde{\ell}_R^+ \tilde{\ell}_R^-$	$0.52^{+5.2\%}_{-4.8\%}$	$0.60^{+2.0\%+5.1\%}_{-2.0\%-6.3\%}$	$0.59^{+0.0\%+5.2\%}_{-0.3\%-6.3\%}$
	$\tilde{\tau}_1^+ \tilde{\tau}_1^-$	$0.58^{+5.2\%}_{-4.8\%}$	$0.67^{+2.0\%+5.1\%}_{-2.0\%-6.4\%}$	$0.66^{+0.0\%+5.2\%}_{-0.3\%-6.4\%}$
450	$\tilde{\ell}_L^+ \tilde{\ell}_L^-$	$0.81^{+6.0\%}_{-5.4\%}$	$0.93^{+2.1\%+5.1\%}_{-2.1\%-6.5\%}$	$0.92^{+0.0\%+5.3\%}_{-0.2\%-6.5\%}$
	$\tilde{\ell}_R^+ \tilde{\ell}_R^-$	$0.31^{+5.9\%}_{-5.4\%}$	$0.36^{+2.0\%+5.4\%}_{-2.1\%-6.7\%}$	$0.35^{+0.0\%+5.6\%}_{-0.2\%-6.7\%}$
	$\tilde{\tau}_1^+ \tilde{\tau}_1^-$	$0.35^{+5.9\%}_{-5.3\%}$	$0.40^{+2.0\%+5.5\%}_{-2.1\%-6.7\%}$	$0.39^{+0.0\%+5.6\%}_{-0.3\%-6.7\%}$
500	$\tilde{\ell}_L^+ \tilde{\ell}_L^-$	$0.50^{+6.6\%}_{-5.9\%}$	$0.58^{+2.1\%+5.5\%}_{-2.2\%-6.9\%}$	$0.57^{+0.0\%+5.4\%}_{-0.3\%-7.0\%}$
	$\tilde{\ell}_R^+ \tilde{\ell}_R^-$	$0.19^{+6.5\%}_{-5.8\%}$	$0.22^{+2.1\%+5.8\%}_{-2.2\%-7.1\%}$	$0.22^{+0.0\%+5.6\%}_{-0.3\%-7.2\%}$
	$\tilde{\tau}_1^+ \tilde{\tau}_1^-$	$0.22^{+6.5\%}_{-5.8\%}$	$0.25^{+2.1\%+5.9\%}_{-2.2\%-7.1\%}$	$0.24^{+0.0\%+5.8\%}_{-0.3\%-7.2\%}$

Table 4. Same as Table 3, but for a center-of-mass energy of 14 Tev.

[11] **ATLAS Collaboration**, *Search for direct-slepton and direct-chargino production in final*

states with two opposite-sign leptons, missing transverse momentum and no jets in 20/fb of pp collisions at $\sqrt{s} = 8$ tev with the atlas detector, ATLAS-CONF-2013-049 (May, 2013).

- [12] **CMS Collaboration**, S. Chatrchyan et al., *Search for electroweak production of charginos and neutralinos using leptonic final states in pp collisions at $\sqrt{s} = 7$ TeV*, *JHEP* **1211** (2012) 147, [[arXiv:1209.6620](#)].
- [13] **CMS Collaboration**, S. Chatrchyan et al., *Search for anomalous production of multilepton events in pp collisions at $\sqrt{s} = 7$ TeV*, *JHEP* **1206** (2012) 169, [[arXiv:1204.5341](#)].
- [14] **CMS Collaboration**, S. Chatrchyan et al., *Search for Physics Beyond the Standard Model Using Multilepton Signatures in pp Collisions at $\sqrt{s} = 7$ TeV*, *Phys.Lett.* **B704** (2011) 411–433, [[arXiv:1106.0933](#)].
- [15] **CMS Collaboration**, *Search for direct EWK production of SUSY particles in multilepton modes with 8TeV data*, *CMS-PAS-SUS-12-022*.
- [16] **CMS Collaboration**, *Search for electroweak production of charginos, neutralinos, and sleptons using leptonic final states in pp collisions at 8 tev*, *CMS-PAS-SUS-13-006* (2013).
- [17] M. E. Krauss, B. O’Leary, W. Porod, and F. Staub, *Implications of gauge kinetic mixing on Z' and slepton production at the LHC*, *Phys.Rev.* **D86** (2012) 055017, [[arXiv:1206.3513](#)].
- [18] M. Frank, L. Selbuz, and I. Turan, *Neutralino and Chargino Production in $U(1)'$ at the LHC*, [[arXiv:1212.4428](#)].
- [19] A. Bharucha, S. Heinemeyer, and F. von der Pahlen, *Direct Chargino-Neutralino Production at the LHC: Interpreting the Exclusion Limits in the Complex MSSM*, [[arXiv:1307.4237](#)].
- [20] A. Alloul, M. Frank, B. Fuks, and M. Rausch de Traubenberg, *Chargino and neutralino production at the Large Hadron Collider in left-right supersymmetric models*, *JHEP* **1310** (2013) 033, [[arXiv:1307.5073](#)].
- [21] D. G. Cerdeno, P. Ghosh, C. B. Park, and M. Peiro, *Collider signatures of a light NMSSM pseudoscalar in neutralino decays in the light of LHC results*, [[arXiv:1307.7601](#)].
- [22] J. D’Hondt, K. De Causmaecker, B. Fuks, A. Mariotti, K. Mawatari, et al., *Multilepton signals of gauge mediated supersymmetry breaking at the LHC*, [[arXiv:1310.0018](#)].
- [23] S. Dawson, E. Eichten, and C. Quigg, *Search for Supersymmetric Particles in Hadron - Hadron Collisions*, *Phys.Rev.* **D31** (1985) 1581.
- [24] H. Baer, C.-h. Chen, F. Paige, and X. Tata, *Detecting Sleptons at Hadron Colliders and Supercolliders*, *Phys.Rev.* **D49** (1994) 3283–3290, [[hep-ph/9311248](#)].
- [25] G. Bozzi, B. Fuks, and M. Klasen, *Slepton production in polarized hadron collisions*, *Phys.Lett.* **B609** (2005) 339–350, [[hep-ph/0411318](#)].
- [26] G. Bozzi, B. Fuks, B. Herrmann, and M. Klasen, *Squark and gaugino hadroproduction and decays in non-minimal flavour violating supersymmetry*, *Nucl.Phys.* **B787** (2007) 1–54, [[arXiv:0704.1826](#)].
- [27] J. Debove, B. Fuks, and M. Klasen, *Model-independent analysis of gaugino-pair production in polarized and unpolarized hadron collisions*, *Phys.Rev.* **D78** (2008) 074020, [[arXiv:0804.0423](#)].
- [28] E. L. Berger, M. Klasen, and T. M. Tait, *Associated production of gauginos and gluinos at hadron colliders in next-to-leading order SUSY QCD*, *Phys.Lett.* **B459** (1999) 165–170, [[hep-ph/9902350](#)].

- [29] W. Beenakker, M. Klasen, M. Kramer, T. Plehn, M. Spira, et al., *The Production of charginos / neutralinos and sleptons at hadron colliders*, *Phys.Rev.Lett.* **83** (1999) 3780–3783, [[hep-ph/9906298](#)].
- [30] E. L. Berger, M. Klasen, and T. M. Tait, *Next-to-leading order SUSY QCD predictions for associated production of gauginos and gluinos*, *Phys.Rev.* **D62** (2000) 095014, [[hep-ph/0005196](#)].
- [31] M. Spira, *Higgs and SUSY particle production at hadron colliders*, [hep-ph/0211145](#).
- [32] G. Bozzi, B. Fuks, and M. Klasen, *Transverse-momentum resummation for slepton-pair production at the CERN LHC*, *Phys.Rev.* **D74** (2006) 015001, [[hep-ph/0603074](#)].
- [33] G. Bozzi, B. Fuks, and M. Klasen, *Threshold Resummation for Slepton-Pair Production at Hadron Colliders*, *Nucl.Phys.* **B777** (2007) 157–181, [[hep-ph/0701202](#)].
- [34] G. Bozzi, B. Fuks, and M. Klasen, *Joint resummation for slepton pair production at hadron colliders*, *Nucl.Phys.* **B794** (2008) 46–60, [[arXiv:0709.3057](#)].
- [35] J. Debove, B. Fuks, and M. Klasen, *Transverse-momentum resummation for gaugino-pair production at hadron colliders*, *Phys.Lett.* **B688** (2010) 208–211, [[arXiv:0907.1105](#)].
- [36] J. Debove, B. Fuks, and M. Klasen, *Threshold resummation for gaugino pair production at hadron colliders*, *Nucl.Phys.* **B842** (2011) 51–85, [[arXiv:1005.2909](#)].
- [37] J. Debove, B. Fuks, and M. Klasen, *Joint Resummation for Gaugino Pair Production at Hadron Colliders*, *Nucl.Phys.* **B849** (2011) 64–79, [[arXiv:1102.4422](#)].
- [38] B. Fuks, M. Klasen, D. R. Lamprea, and M. Rothering, *Gaugino production in proton-proton collisions at a center-of-mass energy of 8 TeV*, *JHEP* **1210** (2012) 081, [[arXiv:1207.2159](#)].
- [39] B. Fuks, M. Klasen, D. R. Lamprea, and M. Rothering, *Precision predictions for electroweak superpartner production at hadron colliders with Resummino*, *Eur.Phys.J.* **C73** (2013) 2480, [[arXiv:1304.0790](#)].
- [40] G. F. Sterman, *Summation of Large Corrections to Short Distance Hadronic Cross-Sections*, *Nucl.Phys.* **B281** (1987) 310.
- [41] S. Catani and L. Trentadue, *Resummation of the QCD Perturbative Series for Hard Processes*, *Nucl.Phys.* **B327** (1989) 323.
- [42] S. Catani and L. Trentadue, *Comment on QCD exponentiation at large x* , *Nucl.Phys.* **B353** (1991) 183–186.
- [43] E. L. Berger and H. Contopanagos, *The Perturbative resummed series for top quark production in hadron reactions*, *Phys.Rev.* **D54** (1996) 3085–3113, [[hep-ph/9603326](#)].
- [44] N. Kidonakis and G. F. Sterman, *Resummation for QCD hard scattering*, *Nucl.Phys.* **B505** (1997) 321–348, [[hep-ph/9705234](#)].
- [45] E. L. Berger and H. Contopanagos, *Threshold resummation of the total cross-section for heavy quark production in hadronic collisions*, *Phys.Rev.* **D57** (1998) 253–264, [[hep-ph/9706206](#)].
- [46] N. Kidonakis, G. Oderda, and G. F. Sterman, *Threshold resummation for dijet cross-sections*, *Nucl.Phys.* **B525** (1998) 299–332, [[hep-ph/9801268](#)].
- [47] A. Vogt, *Next-to-next-to-leading logarithmic threshold resummation for deep inelastic scattering and the Drell-Yan process*, *Phys.Lett.* **B497** (2001) 228–234, [[hep-ph/0010146](#)].

- [48] M. Kramer, E. Laenen, and M. Spira, *Soft gluon radiation in Higgs boson production at the LHC*, *Nucl.Phys.* **B511** (1998) 523–549, [[hep-ph/9611272](#)].
- [49] S. Catani, D. de Florian, and M. Grazzini, *Higgs production in hadron collisions: Soft and virtual QCD corrections at NNLO*, *JHEP* **0105** (2001) 025, [[hep-ph/0102227](#)].
- [50] A. Kulesza, G. F. Sterman, and W. Vogelsang, *Joint resummation in electroweak boson production*, *Phys.Rev.* **D66** (2002) 014011, [[hep-ph/0202251](#)].
- [51] L. G. Almeida, G. F. Sterman, and W. Vogelsang, *Threshold Resummation for Di-hadron Production in Hadronic Collisions*, *Phys.Rev.* **D80** (2009) 074016, [[arXiv:0907.1234](#)].
- [52] H. Contopanagos and G. F. Sterman, *Principal value resummation*, *Nucl.Phys.* **B419** (1994) 77–104, [[hep-ph/9310313](#)].
- [53] S. Catani, M. L. Mangano, P. Nason, and L. Trentadue, *The Resummation of soft gluons in hadronic collisions*, *Nucl.Phys.* **B478** (1996) 273–310, [[hep-ph/9604351](#)].
- [54] **Particle Data Group**, J. Beringer et al., *Review of Particle Physics (RPP)*, *Phys.Rev.* **D86** (2012) 010001.
- [55] J. Pumplin, D. Stump, J. Huston, H. Lai, P. M. Nadolsky, et al., *New generation of parton distributions with uncertainties from global QCD analysis*, *JHEP* **0207** (2002) 012, [[hep-ph/0201195](#)].
- [56] H.-L. Lai, M. Guzzi, J. Huston, Z. Li, P. M. Nadolsky, et al., *New parton distributions for collider physics*, *Phys.Rev.* **D82** (2010) 074024, [[arXiv:1007.2241](#)].
- [57] J. M. Lindert, F. D. Steffen, and M. K. Trenkel, *Direct stau production at hadron colliders in cosmologically motivated scenarios*, *JHEP* **1108** (2011) 151, [[arXiv:1106.4005](#)].
- [58] A. Martin, W. Stirling, R. Thorne, and G. Watt, *Parton distributions for the LHC*, *Eur.Phys.J.* **C63** (2009) 189–285, [[arXiv:0901.0002](#)].
- [59] **NNPDF Collaboration**, R. D. Ball et al., *A Determination of parton distributions with faithful uncertainty estimation*, *Nucl.Phys.* **B809** (2009) 1–63, [[arXiv:0808.1231](#)].
- [60] **The NNPDF Collaboration**, R. D. Ball et al., *Parton distributions with QED corrections*, [[arXiv:1308.0598](#)].
- [61] J. Alwall, M. Herquet, F. Maltoni, O. Mattelaer, and T. Stelzer, *MadGraph 5 : Going Beyond*, *JHEP* **1106** (2011) 128, [[arXiv:1106.0522](#)].
- [62] T. Sjostrand, S. Mrenna, and P. Z. Skands, *PYTHIA 6.4 Physics and Manual*, *JHEP* **0605** (2006) 026, [[hep-ph/0603175](#)].
- [63] M. L. Mangano, M. Moretti, F. Piccinini, R. Pittau, and A. D. Polosa, *ALPGEN, a generator for hard multiparton processes in hadronic collisions*, *JHEP* **0307** (2003) 001, [[hep-ph/0206293](#)].
- [64] M. L. Mangano, M. Moretti, F. Piccinini, and M. Treccani, *Matching matrix elements and shower evolution for top-quark production in hadronic collisions*, *JHEP* **0701** (2007) 013, [[hep-ph/0611129](#)].
- [65] J. Alwall, S. de Visscher, and F. Maltoni, *QCD radiation in the production of heavy colored particles at the LHC*, *JHEP* **0902** (2009) 017, [[arXiv:0810.5350](#)].
- [66] S. Jadach, Z. Was, R. Decker, and J. H. Kuhn, *The tau decay library TAUOLA: Version 2.4*, *Comput.Phys.Commun.* **76** (1993) 361–380.

- [67] S. Ovin, X. Rouby, and V. Lemaitre, *DELPHES, a framework for fast simulation of a generic collider experiment*, [arXiv:0903.2225](#).
- [68] J.-L. Agram, J. Andrea, E. Conte, B. Fuks, D. GelÃƒf, et al., *Probing top anomalous couplings at the LHC with trilepton signatures in the single top mode*, *Phys. Lett.* **B725** (2013) 123–126, [[arXiv:1304.5551](#)].
- [69] C. Degrande, C. Duhr, B. Fuks, D. Grellscheid, O. Mattelaer, et al., *UFO - The Universal FeynRules Output*, *Comput.Phys.Commun.* **183** (2012) 1201–1214, [[arXiv:1108.2040](#)].
- [70] N. D. Christensen and C. Duhr, *FeynRules - Feynman rules made easy*, *Comput.Phys.Commun.* **180** (2009) 1614–1641, [[arXiv:0806.4194](#)].
- [71] N. D. Christensen, P. de Aquino, C. Degrande, C. Duhr, B. Fuks, et al., *A Comprehensive approach to new physics simulations*, *Eur.Phys.J.* **C71** (2011) 1541, [[arXiv:0906.2474](#)].
- [72] C. Duhr and B. Fuks, *A superspace module for the FeynRules package*, *Comput.Phys.Commun.* **182** (2011) 2404–2426, [[arXiv:1102.4191](#)].
- [73] B. Fuks, *Beyond the Minimal Supersymmetric Standard Model: from theory to phenomenology*, *Int.J.Mod.Phys.* **A27** (2012) 1230007, [[arXiv:1202.4769](#)].
- [74] A. Alloul, N. D. Christensen, C. Degrande, C. Duhr, and B. Fuks, *FeynRules 2.0 - A complete toolbox for tree-level phenomenology*, [arXiv:1310.1921](#).
- [75] E. Conte, B. Fuks, and G. Serret, *MadAnalysis 5, A User-Friendly Framework for Collider Phenomenology*, *Comput.Phys.Commun.* **184** (2013) 222–256, [[arXiv:1206.1599](#)].
- [76] E. Conte and B. Fuks, *MadAnalysis 5: status and new developments*, [arXiv:1309.7831](#).
- [77] M. Cacciari, G. P. Salam, and G. Soyez, *The Anti- $k(t)$ jet clustering algorithm*, *JHEP* **0804** (2008) 063, [[arXiv:0802.1189](#)].
- [78] M. Cacciari, G. P. Salam, and G. Soyez, *FastJet User Manual*, *Eur.Phys.J.* **C72** (2012) 1896, [[arXiv:1111.6097](#)].
- [79] A. Barr, C. Lester, and P. Stephens, *$m(T2)$: The Truth behind the glamour*, *J.Phys.* **G29** (2003) 2343–2363, [[hep-ph/0304226](#)].
- [80] K. T. Matchev and M. Park, *A General method for determining the masses of semi-invisibly decaying particles at hadron colliders*, *Phys.Rev.Lett.* **107** (2011) 061801, [[arXiv:0910.1584](#)].